Oliveira, A. S. F., Shoemark, D. K., Campello, H. R., Wonnacott, S., Gallagher, T., Sessions, R. B., & Mulholland, A. J. (2019). Identification of the Initial Steps in Signal Transduction in the α4β2 Nicotinic Receptor: Insights from Equilibrium and Nonequilibrium Simulations. *Structure*, *27*(7), 1171-1183.e3. https://doi.org/10.1016/j.str.2019.04.008

Identification of the initial steps in signal transduction in the α4β2 nicotinic receptor: insights from equilibrium and nonequilibrium simulations

A. Sofia F. Oliveira,[a,b] Deborah K. Shoemark,[a] Hugo Rego Campello,[b] Susan Wonnacott,[c] Timothy Gallagher,[b] Richard B. Sessions[a1*] and Adrian J. Mulholland[b*]

[a] School of Biochemistry, University of Bristol, Bristol BS8 1DT (United Kingdom)

[b] Centre for Computational Chemistry, School of Chemistry, University of Bristol, Bristol BS8 1TS (United Kingdom)

[c] Department of Biology and Biochemistry, University of Bath, Bath BA2 7AY (United Kingdom)

[1] Lead Contact: Richard B. Sessions (r.sessions@bristol.ac.uk)

*Corresponding author(s): r.sessions@bristol.ac.uk adrian.mulholland@bristol.ac.uk

SUMMARY

Nicotinic acetylcholine receptors (nAChRs) modulate synaptic transmission in the nervous system. These receptors have emerged as therapeutic targets in drug discovery for treating several conditions, including Alzheimer's, pain and nicotine addiction. In this in silico study, we use a combination of equilibrium and nonequilibrium molecular dynamics simulations to map dynamic and structural changes induced by nicotine in the human α4β2 nAChR. They reveal a striking pattern of communication between the extracellular binding pockets and the transmembrane domains (TMDs) and show the sequence of conformational changes associated with the initial steps in this process. We propose a general mechanism for signal transduction for Cys-loop receptors: the mechanistic steps for communication proceed firstly via loop C in the principal subunit and are subsequently transmitted, gradually and cumulatively, to loop F of the complementary subunit, and then to the TMDs via the M2-M3 linker.

INTRODUCTION

Nicotinic acetylcholine receptors (nAChRs) are members of the pentameric ligand-gated ion channel (pLGIC) family and are involved in fast synaptic transmission in the peripheral nervous system and serve a more modulatory function in the CNS (Miller and Smart, 2010; Thompson et al.,

2010; Corringer et al., 2012; Nys et al., 2013; Cecchini and Changeux, 2015; Nemecz et al., 2016). pLGICs are frequently referred to as Cys-loop receptors due to a conserved disulphide bond located close to the interface between the extracellular and the transmembrane domains (Nys et al., 2013; Nemecz et al., 2016). The Cys-loop family includes several other important cation and anion-permeable channels, such as the serotonin (5-HT_3R), glycine (GlyR) and γ-aminobutyric acid type A ($GABA_A$R) receptors (Miller and Smart, 2010; Thompson et al., 2010; Nys et al., 2013; Cecchini and Changeux, 2015; Nemecz et al., 2016). In nAChRs, the endogenous neurotransmitter acetylcholine, as well exogenous agonists such as nicotine, bind to the receptor and induce depolarization by opening the ion channel and thereby allowing a flow of positive ions across the membrane (Cecchini and Changeux, 2015; Dineley et al., 2015). Over the last decades, nAChRs have emerged as important targets in drug discovery for the treatment of several conditions including Alzheimer's, schizophrenia, pain and addiction (Cecchini and Changeux, 2015; Dineley et al., 2015).

Details of the molecular architecture of nAChRs have been revealed for the nAChR from *Torpedo marmorata* by cryo-electron microscopy (Miyazawa et al., 2003; Unwin, 2013) and, more recently, the X-ray (Morales-Perez et al., 2016) and cryo-electron structures (Walsh et al., 2018) of the human α4β2 receptor. Crystallographic studies of several water-soluble acetylcholine binding proteins (AChBPs, e.g. (Brejc et al., 2001; Celie et al., 2004; Celie et al., 2005; Li et al., 2011; Rucktooa et al., 2012; Billen et al., 2012)) have also provided insights into ACh binding, although AChBPs lack an ion channel domain. Considerable progress has been made in structural studies of other family members (for a review see (Pless and Sivilotti, 2018)), with several full-length structures determined of both prokaryotic channels (such as GLIC (Hilf and Dutzler, 2009; Hilf et al., 2010; Pan et al., 2012a; Prevost et al., 2012; Sauguet et al., 2013; Gonzalez-Gutierrez et al., 2013; Mowrey et al., 2013; Sauguet et al., 2014; Nemecz et al., 2017; Menny et al., 2017; Fourati et al., 2018) and ELIC (Hilf and Dutzler, 2008; Zimmermann and Dutzler, 2011; Pan et al., 2012b; Gonzalez-Gutierrez et al., 2012; Spurny et al., 2012; Zimmermann et al., 2012; Spurny et al., 2013; Ulens et al., 2014; Chen et al., 2015; Bertozzi et al., 2016; Nys et al., 2016)) and eukaryotic channels (such as GlyRs (Du et al., 2015; Huang et al., 2015; Huang et al., 2017), $GABA_A$Rs (Miller and Aricescu, 2014; Zhu et al., 2018; Miller et al., 2017; Chen et al., 2018; Phulera et al., 2018; Liu et al., 2018; Masiulis et al., 2019; Laverty et al., 2019) and 5-HT_3Rs (Hassaine et al., 2014; Basak et al., 2018a; Polovinkin et al., 2018; Basak et al., 2018b)). The large set of structures currently available reflects the different states of the receptors and the effect of mutations and gives insight into ligand-receptor interactions. They also hint at conformational transitions mediating signal transduction.

nAChRs are formed of five (identical or non-identical) subunits arranged around a central cation-conducting channel (see Figure 1) (Cecchini and Changeux, 2015; Dineley et al., 2015). Each of the five subunits consists of a large extracellular region, comprised of the lengthy N-terminal domain and the linker between transmembrane spans M2 and M3, a transmembrane domain (TMD) comprised of 4 membrane-spanning helices M1-M4, and a variable intracellular domain (ICD) between M3 and M4. Five TMDs together form the channel that enables ions to cross the membrane (Thompson et al., 2010; Nemecz et al., 2016). The ICD region is mainly formed by the large M3–M4 intracellular loop and is thought to be responsible for the regulation and trafficking of the receptor (Thompson et al., 2010; Nemecz et al., 2016). The ECDs contain the ligand-binding pockets, which range between two and five per receptor depending on the receptor subtype (Thompson et al., 2010; Nemecz et al., 2016). The ligand binding pockets are located at the interface between neighbouring subunits and are formed by loops A, B, and C located in the principal side and D, E and F in the complementary side (Figure 1). Each binding pocket (Figure 1) is lined by several aromatic residues (e.g. Y100, W156, Y197, Y204 in the principal subunit and W57, F119 and L121 in the complementary subunit of the human $(\alpha4)_2(\beta2)_3$ receptor (Morales-Perez et al., 2016)), many of which are highly conserved across the Cys-loop family (Nys et al., 2013).

Figure 1

The α4β2 nAChR (the focus of this work) is important from a therapeutic point of view because it is the major nAChR in the brain with high affinity for nicotine (comprising 90% of high-affinity nicotine binding sites in the brain (Dineley et al., 2015)) and hence is key to nicotine addiction. As a consequence, this receptor subtype is the primary target of several smoking cessation drugs, notably varenicline (Hays and Ebbert, 2008) and cytisine (Etter, 2006). Structural studies have revealed vital features of the molecular mechanisms underlying the function of this receptor (Miller and Smart, 2010; Thompson et al., 2010; Nys et al., 2013; Cecchini and Changeux, 2015), but fundamental questions remain. In particular, what are the nicotine-induced conformational changes in the protein and how are these rearrangements transmitted from the ECDs to the TMDs, resulting in the opening of the ion channel? Answering this question requires knowledge of the dynamics of the protein and the identification of the conformational changes that take place upon ligand binding (Amaro and Mulholland, 2018). Grosman *et al.* (Grosman et al., 2000b), using rate equilibrium linear free-energy relationships analysis, proposed a possible pathway connecting the closed and open conformations of the muscle nAChR and suggested that the transmission of conformational changes proceeds in a wave-like manner from the binding site to the TMD (Grosman et al., 2000b). Molecular dynamics (MD) simulations offer a highly effective method to identify, ‘assay’ and

analyse functionally important motions of proteins (e.g. (Oliveira et al., 2011; Woods et al., 2013; Wells et al., 2015; Huggins et al., 2018; Amaro et al., 2018)). The use of nonequilibrium MD simulations (Hoover and Hoover, 2005) is less common (e.g. (Jensen et al., 2002; de Groot et al., 2003; De Fabritiis et al., 2008; Kutzner et al., 2011; Ngo et al., 2014; Ngo et al., 2016; Buchenberg et al., 2017; Stock and Hamm, 2018)) but potentially allows for the characterization of the fast conformational changes occurring in a system as a response to a perturbation (e.g., (Oliveira et al., 2005; Damas et al., 2011)). Several studies using MD simulations (in some cases combined with docking approaches) have been reported for approximate models of the α4β2 nAChR (e.g. (Haddadian et al., 2008; Sgrignani et al., 2009; Cheng et al., 2009a; Liu et al., 2009; Law and Lightstone, 2009; Liu et al., 2010b; Liu et al., 2010a; Willenbring et al., 2010; Beissner et al., 2012; Arias et al., 2013a; Arias et al., 2013b; Arias et al., 2015a; Arias et al., 2015b; Suresh and Hung, 2016; Alcaino et al., 2017)). These studies aimed to understand receptor-ligand interactions and how ligand binding is linked to the cooperative movements in gating. However, as far as we are aware, all the previous studies (both for the isolated domains and for the complete receptor) used homology models as the starting point for the simulations. These models were based on a wide variety of template structures, such as the cryo-EM *Torpedo marmorata* nAChR (Miyazawa et al., 2003) or the acetylcholine binding proteins from *Capitella teleta* (Billen et al., 2012), *Aplysia californica* (Celie et al., 2005) and *Lymnaea stagnalis* (Celie et al., 2004). Furthermore, previous simulations were on the timescale of a few nanoseconds (e.g., ranging from five to tens of ns) and so too short to capture the conformational changes induced by ligands.

Insights into the conformational transitions associated with gating and signal propagation within the Cys-loop family have been provided by MD simulations studies of other Cys-loop receptors (e.g., in the ELIC (Cheng et al., 2009b), GLIC (Nury et al., 2010; Mowrey et al., 2013; Lev et al., 2017), GlyR (Murail et al., 2011; Yu et al., 2014) and GluR (Calimet et al., 2013; Yoluk et al., 2015)). Particularly interesting is the recent work by Lev *et al.,* in which a combination of targeted MD and swarm-based string method simulations were used to identify the molecular events and the energetics of pH activation, ECD-TMD communication, and gating in the bacterial homologue GLIC channel (Lev et al., 2017). That work showed that deprotonation of the aspartate and glutamate residues located at the subunit interface induces the ECD conformational change during channel closure and that the D32-R192 salt bridge is a key interaction in the direct communication between the ECD and the TMD (Lev et al., 2017).

Here, we report an in silico study where we have performed extensive equilibrium MD simulations (totalling 5 μs) of the human α4β2 nAChR using the recently solved crystal structure (Morales-Perez et al., 2016), with and without nicotine in the binding sites. The simulations identify agonist-

induced conformational changes and show how the ligand modulates the receptor dynamics. We have also performed an extensive complementary set of nonequilibrium MD simulations (totalling 2 μs), which reveal the ECD-TMD communication mechanism. This combination of equilibrium and nonequilibrium MD simulations provides a powerful tool to study signal transduction in proteins that should be widely applicable for use in other allosteric systems.

RESULTS AND DISCUSSION

Simulations of the nicotine complex and the apo form

We performed extensive simulations of the free (APO) and nicotine-bound (NCT) systems (with ten replicates of each system) comprising the human α4β2 nAChR inserted into an explicit lipid membrane and solvent. Both systems remain stable over the simulation time (250 ns), and the average C_α root mean square deviation (RMSD) profiles show a plateau after 50 ns (Figure S1). The stability of the systems is further demonstrated by the analysis of the secondary structure of the receptor (in both systems, the protein secondary structure remains intact during the 250 ns, with an average secondary structure loss below 2% using DSSP (Kabsch and Sander, 1983)) (Figure S1). Principal component analysis (PCA) was also used to check the equilibration/relaxation and sampling of the replicates (Roy and Laughton, 2010; Garton and Laughton, 2013; Ng et al., 2013). All replicates were equilibrated after 50 ns. As expected, PCA showed that the different replicates explore different regions of conformational space (Figure S1), thus improving the overall sampling for each system. The use of replicates has been shown to improve sampling compared with a single long simulation (Caves et al., 1998; Perez et al., 2016; Huggins et al., 2018).

In the NCT system, both nicotine molecules (one in each binding pocket) maintained their positions throughout the simulations. The two canonical interactions between the protonated pyrrolidine nitrogen of nicotine and TrpB (W156 from the α4 subunits) (Dougherty, 2008; Tavares Xda et al., 2012; Van Arnam and Dougherty, 2014) are almost always present in both binding pockets. Although the two nicotine molecules are relatively immobile in each site, their behaviour differs to some extent, on the simulated timescale. The analysis of the dihedral angle ϕ between the pyridine and pyrrolidine rings of nicotine showed two persistent conformations resulting in two possible binding modes: a preferred one ($\phi \approx -65^o$) observed in 90% of cases (similar to the binding mode in the X-ray structure (Morales-Perez et al., 2016)) and a second ($\phi \approx 125^o$) observed for the remaining 10%.

Nicotine-induced structural and dynamical changes

Binding of nicotine is thought to induce structural and dynamical changes in the receptor. Root Mean Square Fluctuation (RMSF) profiles of the C_α atoms were calculated for the APO and NCT systems to identify and characterise such changes. The RMSF behaviour among the replicates is very diverse for both the APO and NCT systems (Figure S1). However, despite this diversity, the average RMSF profiles for the APO and the NCT systems are very similar (Figure 2 and S2), indicating that the overall dynamics of the two systems are generally very similar. The only exception is the loop C region of the α4 subunits which shows a significant decrease in flexibility in the nicotine complexes, compared with the apo form. This is in agreement with experimental evidence (particularly from X-ray and Trp fluorescence studies) showing that loop C is relatively disordered, adopting multiple conformations in the absence of a ligand (e.g. (Gao et al., 2005; Ulens et al., 2009; Nys et al., 2013)) and that its conformation becomes restricted upon ligand binding (e.g. (Celie et al., 2005; Gao et al., 2005; Gao et al., 2006; Brams et al., 2011; Unwin and Fujiyoshi, 2012; Nys et al., 2013)). Likewise, several previous MD studies on different pLGICs have also indicated an increase in the flexibility of this loop when no ligand is present in the binding pocket (e.g. (Law et al., 2005; Amiri et al., 2007; Haddadian et al., 2008; Mallipeddi et al., 2013; Naveh et al., 2014; Yoluk et al., 2015)).

Figure 2

To identify nicotine-induced conformational changes, the C_α positional deviations between the APO and the NCT systems were calculated as a function of the residue number for the last 10 ns of simulation (Figures 3).

Figure 3

The final deviation values correspond to the average obtained over all 100 combinations (resulting from the 10 APO × 10 NCT pairs of trajectories). Overall, this approach is a straightforward way to identify the residues that show structural differences between the two systems. The C_α positional deviations were mapped onto the average APO structure in order to identify the residues that undergo the largest relative displacements (Figure 4 and Figure S3).

Figure 4

Overall, the most pronounced conformational differences between the NCT and the APO systems are located in external and flexible regions of the receptor such as the MX-M4 linkers, loop C from

the β2 subunits and the C-termini. All these regions are flexible (Figure 2 and S2), hence caution must be exercised when assessing the relevance of such differences in respect of ligand gating. It should also be noted that the ICDs located between the MX-M4 helices were not modelled (see STAR Methods), thus the differences observed in the MX-M4 loops may have been artificially enhanced by the absence of this domain. Nevertheless, an interesting observation from Figure 4B and Figure S3 is the fact that, in the binding pocket region, the conformational differences between the two systems are subtle and localized in the loop C and TrpB region of the α4 subunit. Loop C forms the outer face of the binding pocket (see Figure 1) and, in our APO simulations, this region displays significant conformational variability (Figure S4). In some APO replicates, this loop moved inward into the binding pocket (Figure S4B), whereas in other cases, it rotated outward (Figure S4C) exposing the binding pocket region to the solvent. Such outward movements are known to be important for the opening of the binding pocket and to allow ligand diffusion in and out of the pocket (Nys et al., 2013).

In the β2 subunit (Figure 4 and S3), the largest conformational differences between the two systems are located in loop F (between D170 and D171) and in the second layer of residues (between A98-F106). Loop F is located at the bottom of the binding pocket (Nys et al., 2013) and, based on available structural and functional data, it has been hypothesized that this loop may have two distinct regions (for a review see (Nys et al., 2013)): the upper part is thought to be important for ligand binding affinity and specificity while the lower part has been proposed to have a direct role in channel gating and in linking binding pocket structural changes to the TMD gate. While the involvement of this loop in ligand binding in the Cys-loop receptor family has been confirmed by voltage-clamp fluorometry experiments (e.g. (Pless and Lynch, 2009; Khatri et al., 2009)), its role in signal transduction and activation (Newell and Czajkowski, 2003; Thompson et al., 2006) remains unclear.

The largest nicotine-induced deviations in the interface between the ECD and TMD domains (Figure 4C and Figure S3C) are located in three distinct regions: the M2-M3 and Cys loops from the α4 subunit and the lower part of loop F from the β2 subunit. The extracellular M2-M3 region is located at the interface between the ECD and the TMDs and has been shown experimentally to be involved in channel gating (e.g. (CamposCaro et al., 1996; Rovira et al., 1998; Grosman et al., 2000a)). Mutations in this loop influence gating and disrupt the link between ligand binding and channel activation (Grosman et al., 2000a; Jha et al., 2007; Bafna et al., 2008). Some of these mutations are also known to cause several human diseases, such as congenital myasthenic syndromes (e.g. (Croxen et al., 1997)). Previous MD simulations of several Cys-loop members (e.g.

(Haddadian et al., 2008; Cheng et al., 2009b; Zhu and Hummer, 2010)) have also suggested that this loop is the main coupling element between the ECDs and the TMDs. The Cys loop of the α4 subunit is one of the most highly conserved structural motifs in the nAChRs family (Le Novere and Changeux, 2001) and is located at the junction between the ECD and TMD (Figure 1). Mutations in this region have a profound effect on ligand binding and attenuate channel gating (Shen et al., 2003).

No significant conformational differences were observed between the NCT and APO systems in the ion permeation pore, not even in the M2 region of the channel. The M2 helices form the inner wall of the ion pore, and their motion directly impacts on pore shape. Therefore, the distances between these helices (Figure S5) were monitored together with the channel profile (data not shown). The receptor ion channel had a V-shaped conformation at the beginning of the simulations with a constriction on the cytoplasmic side of the membrane, mainly due to the position of the side-chains of E247 (α4 subunits) and E239 (β2 subunits) (see Figures 5A and S5). However, during the simulation, the M2 helices underwent a significant reorganisation leading to the closure of the ion channel (Figure 5B). This rearrangement was observed in almost all replicates in both the APO and NCT systems (19 out of the 20 simulations performed) where straightening of the helices occurred exclusively in the M2 extracellular regions (Figure S5B-S5C). The M2 intracellular region showed almost no change during the simulation (Figure S5). Several previous simulation studies with various pLGICs (such as the human α7 nAChR or the nicotinic receptor homologue GLIC) have shown similar straightening motions of the upper region of the M2 helices (e.g. (Nury et al., 2010; Chiodo et al., 2017)) and such tilting/straightening motions are thought to be essential for the opening/closing of the ion channel.

Membrane properties were also monitored along the simulation time using the GridMAT tool (Allen et al., 2009). No major changes in the membrane were observed in the APO and NCT systems. Despite some fluctuations, the membrane remained in the liquid crystalline state and the area per lipid stayed close to the experimental values (Kucerka et al., 2005).

Figure 5

Inter-domain communication and signal transduction

We also performed 400 short nonequilibrium simulations (a total of 2 μs) to study signal transmission from the binding pocket to the ion channel. These short nonequilibrium simulations started from conformations extracted from the equilibrated part (40 conformations per replicate) of the long NCT simulations (Figure 7). In each short simulation, the nicotine molecules were

annihilated in the binding pockets, and the trajectory of these artificial APO systems (containing the receptor, membrane, solvent, and ions) was followed for 5 ns. The subtraction technique (Ciccotti et al., 1979; Paolini et al., 1990) was used to compare the short APO and NCT simulations (Figure S6) and identify the residues involved in signal transmission by cancelling the noise coming from the intrinsic fluctuations of the systems. This approach allows for the identification of the receptor response to instantaneous removal of nicotine from both binding pockets (Figure 6 and Figure S6-S7) and provides a detailed understanding of the associated conformational changes by averaging the difference in the position of the residues between the short APO and NCT simulations at specific time points (Movie 2). Every 0.01 ns the Cα coordinates of each residue in the APO simulation was subtracted from the corresponding Cα atom coordinates of the NCT simulation giving a difference trajectory for this pair of simulations. These difference trajectories were averaged over the set of 400 pairs of short simulations and the standard deviations calculated. Low standard deviations for the average Cα positional deviation between the two states were observed, indicating the significance and reproducibility of the results. It should be noted that these nonequilibrium simulations were designed to force signal transmission in the receptor and thus identify the initial steps in the chain of conformational rearrangements associated with signal propagation. Due to the artificial nature of the perturbation (the creation of a local vacuum upon nicotine annihilation), the response of the system observed here is faster than its response in a biological context. We emphasise that these simulations are not intended to model the physical process of ligand unbinding and the timescale of structural changes in that process or the transitions between states associated with gating; instead, they identify the structural response to the perturbation and the routes by which they are transmitted in the protein. Only the small amplitude conformational changes (associated with the first steps of signal transmission) will be observed, due to the short timescale of the nonequilibrium simulations (5 ns). The large amplitude conformational rearrangements necessary to allow channel opening/closing will not be completely sampled (see Figure S6). Nevertheless, we suggest that such conformational rearrangements occurring between open, resting, intermediate and closed states are likely to involve structural elements of the communication pathway revealed by the nonequilibrium simulations.

Figure 6

These simulations clearly identify common features of structural response to nicotine removal. As can be seen in Figure 6 and Figures S7, fifty picoseconds after nicotine removal, the loop C region from the α4 subunit (residues E198-E202) was the only region in the binding pockets that underwent a conformational change. Notably, the α1-β1 and the β2-β3 loops, which are located at

the top of the receptor and relatively distant (more than 20 Å away) from the binding pockets, also responded rapidly to nicotine removal. Over the next few nanoseconds, a gradual and cumulative increase in the deviations was observed in specific regions of the receptor, mainly in loop F (residues S175-E177) from the β2 subunit and in loops C and M2-M3 (residues T273-P278) from the α4 subunit (see Movie 3). Also, and perhaps surprisingly, the Cys loop showed hardly any rearrangement in response to ligand removal. However, it is important to note that the conformational changes after 5 ns are still far from those observed in the long simulations (Figure S6), meaning, that signal transduction in this receptor is a comparatively slow process and that most of the conformational rearrangements occur long after the initial perturbation. The only exception to this slow response behaviour is the loop C region, which responds rapidly, showing a deviation after 5 ns comparable with that found in the equilibrium simulations.

The results from this nonequilibrium analysis correlate well with the experimental evidence showing that loops C, F, and M2-M3 are involved in ligand binding and/or signal transduction: mutations in the M2-M3 loop in the α subunit modulate communication between the ECD and the TMD (Grosman et al., 2000a; Jha et al., 2007; Bafna et al., 2008) and, in some cases, impair channel gating (Grosman et al., 2000a). Moreover, insertion or a deletion of a residue in this region increases or decreases, respectively, the open-channel lifetimes (Grosman et al., 2000a). Voltage-clamp fluorometry experiments have demonstrated that in Cys-loop receptors (e.g. (Pless and Lynch, 2009; Khatri et al., 2009)), the loop F from the β subunit is essential to ligand binding. Some studies have also suggested that this loop may be involved in signal transduction and channel gating (e.g. (Newell et al., 2004; Padgett and Lummis, 2008)). Loop C has been shown to be involved in agonist binding (e.g. (Jadey and Auerbach, 2012; Purohit and Auerbach, 2013)). However, there is still no consensus regarding how the loop C dynamics is correlated with channel opening (for a detailed review see (Nys et al., 2013)).

Concluding remarks

A combination of equilibrium and nonequilibrium MD simulations here have identified key features of the structural mechanism by which a ligand unbinding event in the ECD of nAChRs is communicated to the TMDs. The results are consistent with experimental structural and mutagenesis studies which have previously identified key residues. By simulation, we have been able to detect and visualise *in silico* the initial steps of these dynamic rearrangements, which propagate the signal through the receptor. We used a combination of extensive (microsecond) equilibrium and nonequilibrium MD simulations to study the dynamical behaviour of the human α4β2 receptor with and without nicotine to identify agonist-induced conformational changes. The

equilibrium simulations show that the structural rearrangements induced by the ligand are not restricted to the binding pocket. Significant nicotine-induced conformational changes are observed in the inter-domain interfaces, mainly in the Cys and M2-M3 loops and in the lower part of loop F. The nonequilibrium simulations identify the initial steps of the inter-domain communication mechanism and the ordering of the conformational changes associated with this process. These simulations show a striking pattern of through-receptor communication, showing the structural pathway involved in signal transmission. Crucially, the conformational steps observed on nicotine deletion proceed firstly via loop C in the α4 subunit, accumulating to impact the loop F of the neighbouring β2 subunit (upper part first, then lower) before proceeding to the TMDs via the M2-M3 linker. Understanding the nAChR communication mechanism in atomic detail should help to explain how some known modulators (such as 5-HI (Zwart et al., 2002)) or NS1738 (Timmermann et al., 2007)) exert their effects, and clarify the role of some structural motifs. It may also assist in the design of new modulators that influence the ECD-TMD signal transduction.

All known Cys-loop receptors share a conserved molecular architecture, despite limited sequence identity (Corringer et al., 2012; Nys et al., 2013). They probably also all share the same communication mechanism: e.g., chimeric Cys-loop receptors formed by modular combinations of the extracellular agonist-binding domains and functionally diverse transmembrane ion channels are functional (Eisele et al., 1993; Grutter et al., 2005; Magnus et al., 2011). Furthermore, mutational studies have also revealed the importance of loops C, Cys, F and M2-M3 in ligand binding, signal transduction and in inter-domain communication in nAChR (e.g. (CamposCaro et al., 1996; Rovira et al., 1998; Grosman et al., 2000a; Shen et al., 2003; Jha et al., 2007; Bafna et al., 2008)) as well in other Cys-loop members (e.g. (Newell and Czajkowski, 2003; Thompson et al., 2006; Newell et al., 2004; Padgett and Lummis, 2008; Pless and Lynch, 2009; Khatri et al., 2009). Combining the experimental data available with the computational work presented here, we suggest that the essential details of the inter-domain communication process identified by our simulations represent a general mechanism for the initial steps in signal transduction for this family of ion channels (see Movie 4).

ACKOWLEDGEMENTS

We thank EPSRC (EP/N024117/1) for financial support. This work was carried out using the computational facilities of the Advanced Computing Research Centre, University of Bristol (http://www.bris.ac.uk/acrc). AJM also thanks EPSRC for funding for CCP-BioSim, the UK Collaborative Computational Project on Biomolecular Simulation (ccpbiosim.ac.uk) under grant number EP/M022609/1. We also thank Oracle for the provision of cloud computing resources.

AUTHORS CONTRIBUTIONS

Conceptualization, A.S.F.O., R.B.S. and A.J.M.; Methodology, A.S.F.O. and R.B.S.; Investigation, A.S.F.O.; Writing – Original Draft, A.S.F.O. and R.B.S.; Writing – Review & Editing, D.K.S., H.R.C., S.W., T.G. and A.J.M.; Funding Acquisition, R.B.S, A.J.M. and T.G.; Supervision, R.B.S., and A.J.M.

DECLARATION OF INTEREST

The authors declare no competing interests.

MAIN FIGURE TITLES AND LEGENDS

Figure 1. X-Ray crystal structure of the human α4β2 receptor (PDB code: 5KXI (Morales-Perez et al., 2016)). **(A)** Architecture of the α4β2 receptor formed by two α4 (coloured in green) and three β2 subunits (coloured in orange). **(B)** Detailed view of the individual α4 and the β2 subunits. Some important structural motifs are highlighted with the following colour scheme: M2-M3 loop, yellow; Cys loop, red; *β1-β2* loop, pink; loop F, magenta; loop C, blue; loop A, orange; loop E, green. **(C)** Chemical structure of (S)-nicotine. **(D)** Detailed view of the ligand-binding pocket. In **A** and **D**, (S)-nicotine (in the protonated form) is represented by pale green spheres.

Figure 2. Average change in RMSF between the APO and NCT systems and associated *p*-values (Roy and Laughton, 2010) for α4 (A) and β2 (B) subunits that form the first binding pocket. A Student's *t*-test was used to compare the APO and NCT systems and to assess the significance of the differences (for more details see the STAR Methods). **(C)** Location of the loop C motif. In this image, the protein structure is the crystallographic conformation used as the starting point for the simulations (PDB code: 5KXI (Morales-Perez et al., 2016)). The α4 and β2 subunits are coloured in green and cyan, respectively. Nicotine is represented with spheres whereas the loop C motif is highlighted in red. See also Figure S2.

Figure 3. Average C_α positional deviation between the NCT and the APO system for all five subunits. The average deviation was determined from all 100 combinations (resulting from the 10 APO × 10 NCT pairs of trajectories) of C_α RMSD between the average structures of the two

systems. The vertical lines represent the standard deviation of the mean. The positions of some important structural motifs are highlighted in yellow.

Figure 4. Nicotine-induced conformational changes. (A) Comparison between the NCT and the APO systems for binding pocket 1 (BP1). **(B)** Detailed view of BP1. **(C)** Detailed view of the ECD-TMD interface. The average C_α positional deviation between the two states is mapped on the average APO structure. In this image, both the structure colours and the cartoon thickness are related to the average Cα positional deviation between the NCT and APO systems. The red, thicker, regions show the residues with the largest differences between the NCT and APO systems. For a detailed view of binding pocket 2 (BP2), see Figure S3 in the supplementary material. See also Figure S3.

Figure 5. Ion permeation channel. (A) Ion permeation channel in the X-ray structure used as the starting point for the simulations (PDB code: 5KXI (Morales-Perez et al., 2016)). This structure is thought to represent a desensitised, non-conducting state of the receptor (Morales-Perez et al., 2016). **(B)** Ion permeation channel in a representative snapshot of the closed channel from equilibrium MD simulations. Only the M2 α-helices are depicted in these images for clarity. The *α4* and *β2* subunits are coloured in green and orange, respectively. The side chains of E247 (*α4* subunits) and E239 (*β2* subunits) are represented with sticks. The grey surface corresponds to the internal surface of the ion channel, and it was determined with the program HOLE (Smart et al., 1996). **(C)** Profiles along the channel axis in the TMD region. The blue and green lines correspond to the pore profiles for open (Du et al., 2015) (PDB code: 3JAE) and closed (Du et al., 2015) (PDB code: 3JAD) GlyR channel whereas the red and orange lines to the α4β2 (Morales-Perez et al., 2016) (PDB code: 5KXI) and $GABA_AR$ (Miller and Aricescu, 2014) (PDB code: 4COF) desensitized channel. The black line shows the profile for the representative snapshot of the closed channel obtained from our simulations. The asterisks in Figures **B** and **C** indicate the narrowest part of the channel. See also Figure S5.

Figure 6. ECD-TMD communication pathway. Mapping of the average Cα-positional deviation in 5 ns following nicotine removal from BP1. The C_α deviation between the short APO and the NCT simulations values at specific times (0, 0.05, 0.5, 1, 3 and 5 ns) after removal of nicotine were calculated as a function of the residue number. The final deviation values correspond to the average obtained over all 400 pairs of simulations (see Figure S6). The average deviations are mapped on to the average APO structure at that time, using the colour scheme presented in the scale. The boxes

show the time evolution of the inter-domain interface (details of the deviations around BP1 and BP2 are shown in Figures S7 in the supplementary material and Movie 2). See also Figure S6 and S7.

Figure 7. Scheme of the short non-equilibrium simulations. From the X-ray structure, we started 10 equilibrium MD simulations of the NCT state (orange). Each replicate was 250 ns long. These long NCT simulations (orange) were used to generate starting structures for the short APO simulations (green): conformations were sampled every 5 ns, starting from the 50 ns structures of the long NCT simulations, giving a total of 400 short APO simulations.

STAR METHODS

CONTACT FOR REAGENTS AND RESOURCE SHARING

Further information and requests for resource sharing should be directed to the Lead Contact, namely Richard B. Sessions (r.sessions@bristol.ac.uk).

METHOD DETAILS

Starting Structure

The 3.9 Å resolution crystal structure of the human α4β2 nicotinic receptor (PDB code: 5KXI) (Morales-Perez et al., 2016) was used as the starting point for this work. All the missing loops were modelled with the program MODELLER 9v17 (Sali, 1995) and all the non-natural linkers inserted to promote crystallisation were removed (e.g. the EA linker inserted between F559–S560 in the α4 subunits and between Q420–S421 in the β2 subunits) (Morales-Perez et al., 2016). We recognise that even small loops pose particular challenges for MD simulations (Liao et al., 2018). The MX-M4 intracellular region of the receptor was not modelled. Overall, 20 different models were generated and the one with the lowest value for MODELLER's objective function was selected.

Protonation state of protonatable residues at pH = 7.0

The protonation states of the protonatable residues in the α4β2 receptor were determined using methodologies for studying the thermodynamics of proton binding described in (Baptista and Soares, 2001; Teixeira et al., 2002). These widely used methodologies (see for example (Bashford and Gerwert, 1992; Baptista et al., 1999; Soares et al., 2004; Teixeira et al., 2005; Oliveira et al., 2014)) use a combination of Poisson-Boltzmann (PB) calculations performed with the software MEAD (version 2.2.9) (Bashford and Karplus, 1990; Bashford and Gerwert, 1992; Bashford, 1997)

and Metropolis Monte Carlo (MC) simulations, using the software PETIT (version 1.6) (Baptista and Soares, 2001).

The dielectric constants used for the solvent (ε_{sol}) and for the protein ($\varepsilon_{protein}$) were 80 and 10, respectively (Teixeira et al., 2005). An implicit membrane was introduced in the x-y plane and modelled as a low dielectric ($\varepsilon_{memb} = 4$) slab of 40 Å. The PB/MC calculations were done with steps of 0.2 pH units. Based on the titration curves, almost all glutamates, aspartates, lysines and arginines were found to be charged. Four exceptions were observed, namely K333, R320 and E282 in the α4 subunits and R351 in the β2 subunits, which were found to be neutral. However, all these four residues were positioned in the polar region of the bilayer and close to the water/membrane interface, where they can easily change their conformation and directly interact with the solvent, and thus were considered to be charged.

In the α4 subunits, H9, H68, H305, H306 and H312 were considered neutral whereas H111, H116, H119 and H169 were (positively) charged. In the β2 subunits, H136, H297, H304, H329 and H330 were considered neutral and H10, H46, H86 and H298 were positively charged.

The pKa value for the pyrrolidine N site in nicotine is ~8.0 (Yang and Smetena, 1995) and by this reason, the nicotine molecules were treated as protonated.

Insertion of the receptor into a lipid bilayer

The reconstructed nicotinic receptor was inserted in a pre-equilibrated 1-palmitoyl-2-oleoyl-sn-glycero-3-phosphocholine (POPC) lipid bilayer using LAMBADA and InflateGRO2 (Schmidt and Kandt, 2012), resulting in a membrane-protein system containing 411 lipid molecules. It should be noted that the membrane used here was formed by a single type of lipid (namely POPC) and did not contain e.g. cholesterol. The lipid composition of the membranes has shown experimentally to modulate receptor function (for a review see (Baenziger et al., 2015)) and the presence of cholesterol may not only influence the bulk membrane physical properties (such as thickness, curvature stress and, bilayer ordering) (Lundbaek et al., 2003) but also bind to specific sites within the TMDs of the receptor (e.g. (Jones and McNamee, 1988)). The membrane model should not, however, affect the conclusions on dynamics and structural changes associated with nicotine binding identified here. For this work, two systems were prepared: in the first, no agonist was bound to the receptor (APO) whereas, in the second, the receptor had one nicotine molecule bound in each binding pocket (NCT). Both systems were solvated using TIP3P water molecules (Jorgensen et al., 1983), and an ionic concentration of 0.1 M sodium chloride was used. The total system size was ~275K atoms.

MD Simulations

All MD simulations were performed using the GROMACS (version 5.1.4) package (Berendsen et al., 1995; Van Der Spoel et al., 2005; Abraham et al., 2015) on the University of Bristol High-Performance Computer, BlueCrystal (Phase 4). The Amber ff99SB-ILDN (Lindorff-Larsen et al., 2010) force field was used for the protein and Slipids for POPC (Jambeck and Lyubartsev, 2012a; Jambeck and Lyubartsev, 2012b). The parameters for the protonated nicotine were taken from our previously published work, where the R configuration was chosen for the nitrogen stereocenter (Campello et al., 2018) corresponding to the stereoisomer modelled in the crystal structure (Morales-Perez et al., 2016) and a higher resolution (2.2 Å) AChBP structure (Dawson et al.).

All simulations were performed at the constant temperature of 310 K and the velocity-rescaling thermostat (Bussi et al., 2007) was used, with separate couplings for the solutes (protein, nicotine and lipids) and solvent, using a relaxation time constant of 0.1 ps. A Berendsen barostat (Berendsen et al., 1984) was used to keep the pressure at 1 bar, with a coupling constant of 1.0 ps and an isothermal compressibility of $4.5\times\ 10^{-5}$ bar^{-1}. The pressure was coupled semi-isotropically, resulting in the independent coupling of the lateral P(x+y) and perpendicular (Pz) pressures.

A time step of 2 fs was used for integrating the equations of motion. Non-bonded long-range electrostatic interactions were calculated using the smooth particle mesh Ewald method (Essmann et al., 1995) beyond a 12 Å cutoff. The same 12 Å cutoff was used for the van der Waals interactions with long-range dispersion corrections for the energy and pressure (Allen and Tildesley, 1987). The neighbour lists were updated every 20 steps. All bonds were constrained to their equilibrium lengths with the LINCS algorithm (Hess et al., 1997) except for the water molecules, which were kept rigid with the SETTLE algorithm (Miyamoto and Kollman, 1992).

The two systems (NCT and APO) were energy minimized with the steepest-descent method (Allen and Tildesley, 1987) in order to remove excessive strain by performing 5000 steps of minimization with harmonic restraints applied to all non-hydrogen atoms, followed by further 5000 steps restraining the C_α atoms only, ending with 5000 steps with no restraints.

After the minimisation step, and in order to allow proper repacking of the lipids around the protein, a 25 ns MD relaxation was performed in two steps. First, a 5 ns simulation was performed with position restraints to all non-hydrogen atoms of the protein and ligands, at a constant temperature. Afterwards, an additional 20-ns long simulation was performed with position restraints applied only the protein's C_α atoms. A force constant of 1000 kJ $mol^{-1}nm^{-2}$ was used for all the steps that

included harmonic position restraints. The unrestrained simulations started after these 25 ns of restrained simulations.

In order to mitigate the sampling problem, 10 MD simulations, 250 ns each, were performed for each system, resulting in 5 μs of total simulation time. All replicates were initiated with different sets of random velocities.

It should be noted that the structure used as the starting point for these equilibrium simulations is proposed to be in a desensitised state in which the ion channel adopts a non-conducting conformation (Morales-Perez et al., 2016) despite agonists being present in the binding pockets. The working mechanism of Cys-loop receptors can be minimally represented by a four state MWC allosteric model (for a review see (Nemecz et al., 2016)): three primary states (Resting, Active and Desensitized) and an intermediate state. According to this model, agonist binding induces a structural transition from a closed to an open conformation, followed by the transition to a high affinity, agonist-bound, nonconducting desensitised state. The exit of the agonist from the binding sites returns the receptor to the closed, resting state again. The equilibrium simulations reported here focus on the identification of the conformational changes induced by nicotine during the Desensitized to Resting transition and do not address or try to model how ligand-binding induces channel opening (which corresponds to the Resting to Active transition).

Nonequilibrium MD simulations

We also performed a large number (400) of very short (5 ns) nonequilibrium simulations to characterise rapid conformational changes and to study the interdomain communication mechanism (Figure 7), using a technique applied successfully previously to other systems (Damas et al., 2011; Oliveira et al., 2005). From the equilibrated part of the 250-ns long NCT simulations (from 50-250 ns), conformations were extracted every 5 ns and used as starting points for the short APO simulations (so a total of 40 different conformations per replicate). In each one of the extracted conformations, the nicotine molecules were removed from the binding pockets, and the trajectory of the resulting APO system was followed during 5 ns.

Figure 7

This annihilation of nicotine is <u>not</u> intended to represent the physical process of unbinding: it is to test the effect of this immediate perturbation on the system, via the subtraction technique, introduced by Ciccotti *et al*. (Ciccotti et al., 1979; Paolini et al., 1990). This subtraction technique was used to analyse the simulations (as described previously (Damas et al., 2011; Oliveira et al.,

2005)) and determine the response of the system to the annihilation of nicotine. According to the subtraction technique (Ciccotti et al., 1979; Paolini et al., 1990), the fast response of a system to a perturbation can be directly measured by averaging the difference of a given property (in this case, the position of the C_α atoms) in perturbed (APO) and unperturbed simulations (NCT) at a given time as long as the two simulations are highly correlated and providing that enough data is gathered. In highly correlated systems, the random fluctuations of the systems largely cancel, thus giving the time evolution of the response to the perturbation. For long simulation times and as the correlation between the trajectories is lost, the subtraction technique is no longer useful. It should be noted that these nonequilibrium simulations (due to their short timescales and the artificial nature of the perturbation) are not in any way attempting to explain the entire mechanism of how ligand binding and unbinding induces channel opening and closing. Rather, they allow the identification of the first conformational changes associated with signal propagation through identification of common features. The standard deviation (SD) for the average C_α positional deviation between the APO and NCT systems was determined to test for the significance and reproducibility of the results. Overall, low SD values were observed for all the regions of interest (data not shown).

QUANTIFICATION AND STATISTICAL ANALYSIS

All the analyses were performed using GROMACS tools (Berendsen et al., 1995; Van Der Spoel et al., 2005; Abraham et al., 2015), in-house tools and the program PyMOL (Delano, 2003). The RMSD and RMSF were calculated after least-squares fit to the C_α atoms of the initial structure. The ϕ dihedral between the pyridine and pyrrolidine rings of nicotine was defined using the N2-C6-C2-C1 atoms (according to the X-ray nomenclature (Morales-Perez et al., 2016)). The ion channel diameter profile along time was calculated using the program HOLE (Smart et al., 1996). The membrane properties were determined using the GridMAT tool (Allen et al., 2009). PCA analysis was used to examine the sampling and equilibration of the replicates (similarly to, e.g. (Roy and Laughton, 2010; Garton and Laughton, 2013; Ng et al., 2013)). All replicates for each system were combined before the analysis so that the dynamics of the individual replicates could be directly compared (within a common subspace). Each PCA trajectory contained one conformation per nanosecond per replicate (totaling 2501 frames) with all the C_α atoms of protein. The two principal components (PC1 and PC2) were used to assess the equilibration/relaxation of the simulations, and all systems were considered equilibrated after 50 ns.

A simple Student's *t*-test was used to compare the APO and NCT RMSFs and to assess the significance of the differences observed (similarly to Roy and Laughton, 2010). For this test, the

sample size was 10, and it was assumed that the two samples were independent, the dependent variable was normally distributed and that the variances of the dependent variable were equal.

DATA AND SOFTWARE AVAILABILITY

The data will be shared upon request. Any requests for data sharing should be directed to the Lead Contact, namely Richard B. Sessions (r.sessions@bristol.ac.uk).

SUPPLEMENTAL VIDEOS

Movie 1. Nicotine-induced conformational changes in the α4β2 receptor, Related to Figure 3. The global average structures (obtained over the last 10 ns of simulation of each replicate and averaged over the 10 replicates) for the APO and NCT systems are represented sequentially, allowing us to identify the conformational changes directly induced by nicotine. The α4 and β2 subunits are coloured in green and orange, respectively. The magenta spheres represent the nicotine molecule.

Movie 2. Time evolution of the deviations along the 5 ns after nicotine's deletion from the BP1, Related to Figure 6.

Movie 3. Conformational changes induced by nicotine annihilation in the BP1, Related to Figure 6. The global average structures (obtained after 5 ns and averaged over the 400 short simulations) for the APO and NCT systems are represented sequentially, allowing us to identify the conformational changes directly induced by the removal of nicotine. The α4 and β2 subunits are coloured in green and orange, respectively. The magenta spheres represent the nicotine molecule.

Movie 4. First steps in the proposed communication mechanism for the Cys-loop family, Related to STAR Methods.

REFERENCES

Abraham, M. J., Murtola, T., Schulz, R., Pall, S., Smith, J. C., Hess, B. & Lindahl, E. 2015. GROMACS: High performance molecular simulations through multi-level parallelism from laptops to supercomputers. *SoftwareX,* 1-2, 19-25.

Alcaino, C., Musgaard, M., Minguez, T., Mazzaferro, S., Faundez, M., Iturriaga-Vasquez, P., Biggin, P. C. & Bermudez, I. 2017. Role of the Cys Loop and Transmembrane Domain in the Allosteric Modulation of alpha4beta2 Nicotinic Acetylcholine Receptors. *J Biol Chem,* 292, 551-562.

Allen, M. P. & Tildesley, D. J. 1987. *Computer simulation of liquids*, Oxford, UK: Clarendon Press.

Allen, W. J., Lemkul, J. A. & Bevan, D. R. 2009. GridMAT-MD: A Grid-Based Membrane Analysis Tool for Use With Molecular Dynamics. *J Comput Chem,* 30, 1952-1958.

Amaro, R. E., Ieong, P. U., Huber, G., Dommer, A., Steven, A. C., Bush, R. M., Durrant, J. D. & Votapka, L. W. 2018. A Computational Assay that Explores the Hemagglutinin/Neuraminidase Functional Balance Reveals the Neuraminidase Secondary Site as a Novel Anti-Influenza Target. *ACS Cent Sci,* 4, 1570-1577.

Amaro, R. E. & Mulholland, A. J. 2018. Multiscale methods in drug design bridge chemical and biological complexity in the search for cures. *Nat Rev Chem,* 2, 0148

Amiri, S., Sansom, M. S. P. & Biggin, P. C. 2007. Molecular dynamics studies of AChBP with nicotine and carbamylcholine: the role of water in the binding pocket. *Protein Eng Des Sel,* 20, 353-359.

Arias, H. R., Fedorov, N. B., Benson, L. C., Lippiello, P. M., Gatto, G. J., Feuerbach, D. & Ortells, M. O. 2013a. Functional and structural interaction of (-)-reboxetine with the human alpha4beta2 nicotinic acetylcholine receptor. *J Pharmacol Exp Ther,* 344, 113-123.

Arias, H. R., Feuerbach, D. & Ortells, M. 2015a. Functional and structural interaction of (-)-lobeline with human alpha4beta2 and alpha4beta4 nicotinic acetylcholine receptor subtypes. *Int J Biochem Cell Biol,* 64, 15-24.

Arias, H. R., Feuerbach, D., Targowska-Duda, K., Kaczor, A. A., Poso, A. & Jozwiak, K. 2015b. Pharmacological and molecular studies on the interaction of varenicline with different nicotinic acetylcholine receptor subtypes. Potential mechanism underlying partial agonism at human alpha4beta2 and alpha3beta4 subtypes. *Biochim Biophys Acta,* 1848, 731-741.

Arias, H. R., Lopez, J. J., Feuerbach, D., Fierro, A., Ortells, M. O. & Perez, E. G. 2013b. Novel 2-(substituted benzyl)quinuclidines inhibit human alpha7 and alpha4beta2 nicotinic receptors by different mechanisms. *Int J Biochem Cell Biol,* 45, 2420-2430.

Baenziger, J. E., Henault, C. M., Therien, J. P. & Sun, J. 2015. Nicotinic acetylcholine receptor-lipid interactions: Mechanistic insight and biological function. *Biochim Biophys Acta,* 1848, 1806-1817.

Bafna, P. A., Purohit, P. G. & Auerbach, A. 2008. Gating at the mouth of the acetylcholine receptor channel: energetic consequences of mutations in the alphaM2-cap. *PLoS One,* 3, e2515.

Baptista, A. M., Martel, P. J. & Soares, C. M. 1999. Simulation of electron-proton coupling with a monte carlo method: application to cytochrome c_3 using continuum electrostatics. *Biophys J,* 76, 2978-2998.

Baptista, A. M. & Soares, C. M. 2001. Some theoretical and computational aspects of the inclusion of proton isomerism in the protonation equilibrium of proteins. *J Phys Chem B,* 105, 293-309.

Basak, S., Gicheru, Y., Rao, S., Sansom, M. S. P. & Chakrapani, S. 2018a. Cryo-EM reveals two distinct serotonin-bound conformations of full-length 5-HT3A receptor. *Nature,* 563, 270-274.

Basak, S., Gicheru, Y., Samanta, A., Molugu, S. K., Huang, W., Fuente, M., Hughes, T., Taylor, D. J., Nieman, M. T., Moiseenkova-Bell, V. & Chakrapani, S. 2018b. Cryo-EM structure of 5-HT3A receptor in its resting conformation. *Nat Commun,* 9, 514.

Bashford, D. 1997. An object-oriented programming suite for electrostatic effects in biological molecules. *In:* Ishikawa, Y., Oldehoeft, R. R., Reynders, J. V. W. & Tholburn, M. (eds.) *Scientific Computing in Object-Oriented Parallel Environments.* Berlin: ISCOPE97, Springer.

Bashford, D. & Gerwert, K. 1992. Electrostatic calculations of the pKa values of ionizable groups in bacteriorhodopsin. *J Mol Biol,* 224, 473-486.

Bashford, D. & Karplus, M. 1990. pKa's of ionizable groups in proteins: atomic detail from a continuum electrostatic model. *Biochemistry,* 29**,** 10219-25.

Beissner, M., Dutertre, S., Schemm, R., Danker, T., Sporning, A., Grubmuller, H. & Nicke, A. 2012. Efficient binding of 4/7 alpha-conotoxins to nicotinic alpha4beta2 receptors is prevented by Arg185 and Pro195 in the alpha4 subunit. *Mol Pharmacol,* 82, 711-718.

Berendsen, H., Postma, J., van Gunsteren, W., Dinola, A. & Haak, J. 1984. Molecular dynamics with coupling to an external bath. *J Chem Phys,* 81, 3684-3690.

Berendsen, H. J. C., Vanderspoel, D. & Vandrunen, R. 1995. Gromacs - a Message-Passing Parallel Molecular-Dynamics Implementation. *Comput Phys Commun,* 91, 43-56.

Bertozzi, C., Zimmermann, I., Engeler, S., Hilf, R. J. & Dutzler, R. 2016. Signal Transduction at the Domain Interface of Prokaryotic Pentameric Ligand-Gated Ion Channels. *PLoS Biol,* 14, e1002393.

Billen, B., Spurny, R., Brams, M., van Elk, R., Valera-Kummer, S., Yakel, J. L., Voets, T., Bertrand, D., Smit, A. B. & Ulens, C. 2012. Molecular actions of smoking cessation drugs at alpha4beta2 nicotinic receptors defined in crystal structures of a homologous binding protein. *Proc Natl Acad Sci U S A,* 109, 9173-9178.

Brams, M., Pandya, A., Kuzmin, D., van Elk, R., Krijnen, L., Yakel, J. L., Tsetlin, V., Smit, A. B. & Ulens, C. 2011. A Structural and Mutagenic Blueprint for Molecular Recognition of Strychnine and d-Tubocurarine by Different Cys-Loop Receptors. *Plos Biology,* 9, e1001043

Brejc, K., van Dijk, W. J., Klaassen, R. V., Schuurmans, M., van Der Oost, J., Smit, A. B. & Sixma, T. K. 2001. Crystal structure of an ACh-binding protein reveals the ligand-binding domain of nicotinic receptors. *Nature,* 411, 269-276.

Buchenberg, S., Sittel, F. & Stock, G. 2017. Time-resolved observation of protein allosteric communication. *Proc Natl Acad Sci U S A,* 114, E6804-E6811.

Bussi, G., Donadio, D. & Parrinello, M. 2007. Canonical sampling through velocity rescaling. *J Chem Phys,* 126**,** 014101.

Calimet, N., Simoes, M., Changeux, J. P., Karplus, M., Taly, A. & Cecchini, M. 2013. A gating mechanism of pentameric ligand-gated ion channels. *Proc Natl Acad Sci U S A,* 110, E3987-96.

Campello, H. R., Del Villar, S. G., Honraedt, A., Viñas, T. M., Oliveira, A. S. F., Ranaghan, K. E., Shoemark, D. K., Bermudez, I., Gotti, C., Sessions, R. B., Mulholland, A. J., Wonnacott, S. & Gallagher, T. 2018a. Unlocking Nicotinic Selectivity via Direct C–H Functionalisation of (–)-Cytisine. *Chem,* 4**,** 1710-1725.

CamposCaro, A., Sala, S., Ballesta, J. J., VicenteAgullo, F., Criado, M. & Sala, F. 1996. A single residue in the M2-M3 loop is a major determinant of coupling between binding and gating in neuronal nicotinic receptors. *Proc Natl Acad Sci U S A,* 93, 6118-6123.

Caves, L. S. D., Evanseck, J. D. & Karplus, M. 1998. Locally accessible conformations of proteins: Multiple molecular dynamics simulations of crambin. *Protein Sci,* 7, 649-666.

Cecchini, M. & Changeux, J. P. 2015. The nicotinic acetylcholine receptor and its prokaryotic homologues: Structure, conformational transitions & allosteric modulation. *Neuropharmacology,* 96, 137-149.

Celie, P. H. N., Kasheverov, I. E., Mordvintsev, D. Y., Hogg, R. C., van Nierop, P., van Elk, R., van Rossum-Fikkert, S. E., Zhmak, M. N., Bertrand, D., Tsetlin, V., Sixma, T. K. & Smit, A. B. 2005. Crystal structure of nicotinic acetylcholine receptor homolog AChBP in complex with an alpha-conotoxin PnIA variant. *Nat Struct Mol Biol,* 12, 582-588.

Celie, P. H. N., van Rossum-Fikkert, S. E., van Dijk, W. J., Brejc, K., Smit, A. B. & Sixma, T. K. 2004. Nicotine and carbamylcholine binding to nicotinic acetylcholine receptors as studied in AChBP crystal structures. *Neuron,* 41, 907-914.

Chen, Q., Kinde, M. N., Arjunan, P., Wells, M. M., Cohen, A. E., Xu, Y. & Tang, P. 2015. Direct Pore Binding as a Mechanism for Isoflurane Inhibition of the Pentameric Ligand-gated Ion Channel ELIC. *Sci Rep,* 5, 13833.

Chen, Q., Wells, M. M., Arjunan, P., Tillman, T. S., Cohen, A. E., Xu, Y. & Tang, P. 2018. Structural basis of neurosteroid anesthetic action on GABAA receptors. *Nat Commun,* 9, 3972.

Cheng, M. H., Xu, Y. & Tang, P. 2009a. Anionic lipid and cholesterol interactions with alpha4beta2 nAChR: insights from MD simulations. *J Phys Chem B,* 113, 6964-6970.

Cheng, X., Ivanov, I., Wang, H., Sine, S. M. & McCammon, J. A. 2009b. Molecular-dynamics simulations of ELIC-a prokaryotic homologue of the nicotinic acetylcholine receptor. *Biophys J,* 96, 4502-4513.

Chiodo, L., Malliavin, T. E., Maragliano, L. & Cottone, G. 2017. A possible desensitized state conformation of the human alpha7 nicotinic receptor: A molecular dynamics study. *Biophys Chem,* 229, 99-109.

Ciccotti, G., Jacucci, G. & McDonald, I. R. 1979. Thought-Experiments by Molecular Dynamics. *J Stat Phys,* 21, 1-21.

Corringer, P. J., Poitevin, F., Prevost, M. S., Sauguet, L., Delarue, M. & Changeux, J. P. 2012. Structure and pharmacology of pentameric receptor channels: from bacteria to brain. *Structure,* 20, 941-956.

Croxen, R., Newland, C., Beeson, D., Oosterhuis, H., Chauplannaz, G., Vincent, A. & Newsom-Davis, J. 1997. Mutations in different functional domains of the human muscle acetylcholine receptor alpha subunit in patients with the slow-channel congenital myasthenic syndrome. *Hum Mol Genet,* 6, 767-774.

Damas, J. M., Oliveira, A. S., Baptista, A. M. & Soares, C. M. 2011. Structural consequences of ATP hydrolysis on the ABC transporter NBD dimer: molecular dynamics studies of HlyB. *Protein Sci,* 20, 1220-1230.

Dawson, A., Hunter, W. N., de Souza, J. O. & Trumper, P. Crystal structure of wild type Aplysia californica AChBP in complex with nicotine. *To be published*.

De Fabritiis, G., Coveney, P. V. & Villa-Freixa, J. 2008. Energetics of K+ permeability through Gramicidin A by forward-reverse steered molecular dynamics. *Proteins,* 73, 185-194.

de Groot, B. L., Frigato, T., Helms, V. & Grubmuller, H. 2003. The mechanism of proton exclusion in the aquaporin-1 water channel. *J Mol Biol,* 333, 279-293.

Delano, W. L. 2003. *The Pymol molecular graphics system. version 0.98*, San Carlos, CA, USA: Delano Scientific LLC.

Dineley, K. T., Pandya, A. A. & Yakel, J. L. 2015. Nicotinic ACh receptors as therapeutic targets in CNS disorders. *Trends Pharmacol Sci,* 36, 96-108.

Dougherty, D. A. 2008. Cys-loop neuroreceptors: structure to the rescue? *Chem Rev,* 108, 1642-1653.

Du, J., Lu, W., Wu, S., Cheng, Y. & Gouaux, E. 2015. Glycine receptor mechanism elucidated by electron cryo-microscopy. *Nature,* 526, 224-9.

Eisele, J. L., Bertrand, S., Galzi, J. L., Devillers-Thiery, A., Changeux, J. P. & Bertrand, D. 1993. Chimaeric nicotinic-serotonergic receptor combines distinct ligand binding and channel specificities. *Nature,* 366, 479-483.

Essmann, U., Perera, L. & Berkowitz, M. L. 1995. A smooth particle mesh Ewald method. *J Chem Phys,* 103, 8577-8593.

Etter, J. F. 2006. Cytisine for smoking cessation: a literature review and a meta-analysis. *Arch Intern Med,* 166, 1553-1559.

Fourati, Z., Howard, R. J., Heusser, S. A., Hu, H., Ruza, R. R., Sauguet, L., Lindahl, E. & Delarue, M. 2018. Structural Basis for a Bimodal Allosteric Mechanism of General Anesthetic Modulation in Pentameric Ligand-Gated Ion Channels. *Cell Rep,* 23, 993-1004.

Gao, F., Bren, N., Burghardt, T. P., Hansen, S., Henchman, R. H., Taylor, P., McCammon, J. A. & Sine, S. M. 2005. Agonist-mediated conformational changes in acetylcholine-binding protein revealed by simulation and intrinsic tryptophan fluorescence. *J Biol Chem,* 280, 8443-8451.

Gao, F., Mer, G., Tonelli, M., Hansen, S. B., Burghardt, T. P., Taylor, P. & Sine, S. M. 2006. Solution NMR of acetylcholine binding protein reveals agonist-mediated conformational change of the C-loop. *Mol Pharmacol,* 70, 1230-1235.

Garton, M. & Laughton, C. 2013. A comprehensive model for the recognition of human telomeres by TRF1. *J Mol Biol,* 425, 2910-2921.

Gonzalez-Gutierrez, G., Cuello, L. G., Nair, S. K. & Grosman, C. 2013. Gating of the proton-gated ion channel from Gloeobacter violaceus at pH 4 as revealed by X-ray crystallography. *Proc Natl Acad Sci U S A,* 110, 18716-18721.

Gonzalez-Gutierrez, G., Lukk, T., Agarwal, V., Papke, D., Nair, S. K. & Grosman, C. 2012. Mutations that stabilize the open state of the Erwinia chrisanthemi ligand-gated ion channel fail to change the conformation of the pore domain in crystals. *Proc Natl Acad Sci U S A,* 109, 6331-6336.

Grosman, C., Salamone, F. N., Sine, S. M. & Auerbach, A. 2000a. The extracellular linker of muscle acetylcholine receptor channels is a gating control element. *J Gen Physiol,* 116, 327-340.

Grosman, C., Zhou, M. & Auerbach, A. 2000b. Mapping the conformational wave of acetylcholine receptor channel gating. *Nature,* 403, 773-776.

Grutter, T., de Carvalho, L. P., Dufresne, V., Taly, A., Edelstein, S. J. & Changeux, J. P. 2005. Molecular tuning of fast gating in pentameric ligand-gated ion channels. *Proc Natl Acad Sci U S A,* 102, 18207-18212.

Haddadian, E. J., Cheng, M. H., Coalson, R. D., Xu, Y. & Tang, P. 2008. In silico models for the human alpha4beta2 nicotinic acetylcholine receptor. *J Phys Chem B,* 112, 13981-13990.

Hassaine, G., Deluz, C., Grasso, L., Wyss, R., Tol, M. B., Hovius, R., Graff, A., Stahlberg, H., Tomizaki, T., Desmyter, A., Moreau, C., Li, X. D., Poitevin, F., Vogel, H. & Nury, H. 2014. X-ray structure of the mouse serotonin 5-HT3 receptor. *Nature,* 512, 276-281.

Hays, J. T. & Ebbert, J. O. 2008. Varenicline for tobacco dependence. *N Engl J Med,* 359, 2018-2024.

Hess, B., Bekker, H., Berendsen, H. J. C. & Fraaije, J. G. E. M. 1997. LINCS: a linear constraint solver for molecular simulations. *J Comput Chem,* 18, 1463-1472.

Hilf, R. J., Bertozzi, C., Zimmermann, I., Reiter, A., Trauner, D. & Dutzler, R. 2010. Structural basis of open channel block in a prokaryotic pentameric ligand-gated ion channel. *Nat Struct Mol Biol,* 17, 1330-1336.

Hilf, R. J. & Dutzler, R. 2008. X-ray structure of a prokaryotic pentameric ligand-gated ion channel. *Nature,* 452, 375-379.

Hilf, R. J. & Dutzler, R. 2009. Structure of a potentially open state of a proton-activated pentameric ligand-gated ion channel. *Nature,* 457, 115-118.

Hoover, W. G. & Hoover, C. G. 2005. Nonequilibrium molecular dynamics. *Condensed Matter Physics,* 8, 247-260.

Huang, X., Chen, H., Michelsen, K., Schneider, S. & Shaffer, P. L. 2015. Crystal structure of human glycine receptor-alpha3 bound to antagonist strychnine. *Nature,* 526, 277-280.

Huang, X., Chen, H. & Shaffer, P. L. 2017. Crystal Structures of Human GlyRalpha3 Bound to Ivermectin. *Structure,* 25, 945-950.

Huggins, D. J., Biggin, P. C., Dämgen, M. A., Essex, J. W., Harris, S. A., Henchman, R. H., Khalid, S., Kuzmanic, A., Laughton, C. A., Michel, J., Mulholland, A. J., Rosta, E., Sansom, M. S. P. & van der Kamp, M. W. 2018. Biomolecular simulations: From dynamics and mechanisms to computational assays of biological activity. *WIRES Comput Mol Sci,* e1393, 1-23.

Jadey, S. & Auerbach, A. 2012. An integrated catch-and-hold mechanism activates nicotinic acetylcholine receptors. *J Gen Physiol,* 140, 17-28.

Jambeck, J. P. M. & Lyubartsev, A. P. 2012a. An Extension and Further Validation of an All-Atomistic Force Field for Biological Membranes. *J Chem Theory Comput,* 8, 2938-2948.

Jambeck, J. P. M. & Lyubartsev, A. P. 2012b. Derivation and Systematic Validation of a Refined All-Atom Force Field for Phosphatidylcholine Lipids. *J Phys Chem B,* 116, 3164-3179.

Jensen, M. O., Park, S., Tajkhorshid, E. & Schulten, K. 2002. Energetics of glycerol conduction through aquaglyceroporin GlpF. *Proc Natl Acad Sci U S A,* 99, 6731-6736.

Jha, A., Cadugan, D. J., Purohit, P. & Auerbach, A. 2007. Acetylcholine receptor gating at extracellular transmembrane domain interface: the cys-loop and M2-M3 linker. *J Gen Physiol,* 130, 547-558.

Jones, O. T. & McNamee, M. G. 1988. Annular and nonannular binding sites for cholesterol associated with the nicotinic acetylcholine receptor. *Biochemistry,* 27, 2364-2374.

Jorgensen, W. L., Chandrasekhar, J., Madura, J. D., Impey, R. W. & Klein, M. L. 1983. Comparison of Simple Potential Functions for Simulating Liquid Water. *J Chem Phys,* 79, 926-935.

Kabsch, W. & Sander, C. 1983. Dictionary of protein secondary structure: pattern recognition of hydrogen-bonded and geometrical features. *Biopolymers,* 22, 2577-2637.

Khatri, A., Sedelnikova, A. & Weiss, D. S. 2009. Structural Rearrangements in Loop F of the GABA Receptor Signal Ligand Binding, Not Channel Activation. *Biophys J,* 96, 45-55.

Kucerka, N., Tristram-Nagle, S. & Nagle, J. F. 2005. Structure of fully hydrated fluid phase lipid bilayers with monounsaturated chains. *J Membr Biol,* 208, 193-202.

Kutzner, C., Grubmuller, H., de Groot, B. L. & Zachariae, U. 2011. Computational electrophysiology: the molecular dynamics of ion channel permeation and selectivity in atomistic detail. *Biophys J,* 101, 809-817.

Laverty, D., Desai, R., Uchanski, T., Masiulis, S., Stec, W. J., Malinauskas, T., Zivanov, J., Pardon, E., Steyaert, J., Miller, K. W. & Aricescu, A. R. 2019. Cryo-EM structure of the human alpha1beta3gamma2 GABAA receptor in a lipid bilayer. *Nature,* 565, 516-520.

Law, R. J., Henchman, R. H. & McCammon, J. A. 2005. A gating mechanism proposed from a simulation of a human alpha7 nicotinic acetylcholine receptor. *Proc Natl Acad Sci U S A,* 102, 6813-6818.

Law, R. J. & Lightstone, F. C. 2009. Modeling neuronal nicotinic and GABA receptors: important interface salt-links and protein dynamics. *Biophys J,* 97, 1586-1594.

Le Novere, N. & Changeux, J. P. 2001. LGICdb: the ligand-gated ion channel database. *Nucleic Acids Res,* 29, 294-295.

Lev, B., Murail, S., Poitevin, F., Cromer, B. A., Baaden, M., Delarue, M. & Allen, T. W. 2017. String method solution of the gating pathways for a pentameric ligand-gated ion channel. *Proc Natl Acad Sci U S A,* 114, E4158-E4167.

Li, S. X., Huang, S., Bren, N., Noridomi, K., Dellisanti, C. D., Sine, S. M. & Chen, L. 2011. Ligand-binding domain of an alpha7-nicotinic receptor chimera and its complex with agonist. *Nat Neurosci,* 14, 1253-1259.

Liao, Q., Kulkarni, Y., Sengupta, U., Petrovic, D., Mulholland, A. J., van der Kamp, M. W., Strodel, B. & Kamerlin, S. C. L. 2018. Loop Motion in Triosephosphate Isomerase Is Not a Simple Open and Shut Case. *J Am Chem Soc,* 140, 15889-15903.

Lindorff-Larsen, K., Piana, S., Palmo, K., Maragakis, P., Klepeis, J. L., Dror, R. O. & Shaw, D. E. 2010. Improved side-chain torsion potentials for the Amber ff99SB protein force field. *Proteins,* 78, 1950-1958.

Liu, G. Y., Ju, X. L. & Cheng, J. 2010a. Selectivity of Imidacloprid for fruit fly versus rat nicotinic acetylcholine receptors by molecular modeling. *J Mol Model,* 16, 993-1002.

Liu, L. T., Haddadian, E. J., Willenbring, D., Xu, Y. & Tang, P. 2010b. Higher susceptibility to halothane modulation in open- than in closed-channel alpha4beta2 nAChR revealed by molecular dynamics simulations. *J Phys Chem B,* 114, 626-632.

Liu, L. T., Willenbring, D., Xu, Y. & Tang, P. 2009. General Anesthetic Binding to Neuronal alpha 4 beta 2 Nicotinic Acetylcholine Receptor and Its Effects on Global Dynamics. *J Phys Chem B,* 113, 12581-12589.

Liu, S., Xu, L., Guan, F., Liu, Y. T., Cui, Y., Zhang, Q., Zheng, X., Bi, G. Q., Zhou, Z. H., Zhang, X. & Ye, S. 2018. Cryo-EM structure of the human alpha5beta3 GABAA receptor. *Cell Res,* 28, 958-961.

Lundbaek, J. A., Andersen, O. S., Werge, T. & Nielsen, C. 2003. Cholesterol-induced protein sorting: an analysis of energetic feasibility. *Biophys J,* 84, 2080-2089.

Magnus, C. J., Lee, P. H., Atasoy, D., Su, H. H., Looger, L. L. & Sternson, S. M. 2011. Chemical and genetic engineering of selective ion channel-ligand interactions. *Science,* 333, 1292-1296.

Mallipeddi, P. L., Pedersen, S. E. & Briggs, J. M. 2013. Interactions of acetylcholine binding site residues contributing to nicotinic acetylcholine receptor gating: Role of residues Y93, Y190, K145 and D200. *J Mol Graph Model,* 44, 145-154.

Masiulis, S., Desai, R., Uchanski, T., Serna Martin, I., Laverty, D., Karia, D., Malinauskas, T., Zivanov, J., Pardon, E., Kotecha, A., Steyaert, J., Miller, K. W. & Aricescu, A. R. 2019. GABAA receptor signalling mechanisms revealed by structural pharmacology. *Nature,* 565**,** 454-459.

Menny, A., Lefebvre, S. N., Schmidpeter, P. A., Drege, E., Fourati, Z., Delarue, M., Edelstein, S. J., Nimigean, C. M., Joseph, D. & Corringer, P. J. 2017. Identification of a pre-active conformation of a pentameric channel receptor. *Elife,* 6, e23955

Miller, P. S. & Aricescu, A. R. 2014. Crystal structure of a human GABAA receptor. *Nature,* 512, 270-275.

Miller, P. S., Scott, S., Masiulis, S., De Colibus, L., Pardon, E., Steyaert, J. & Aricescu, A. R. 2017. Structural basis for GABAA receptor potentiation by neurosteroids. *Nat Struct Mol Biol,* 24, 986-992.

Miller, P. S. & Smart, T. G. 2010. Binding, activation and modulation of Cys-loop receptors. *Trends Pharmacol Sci,* 31, 161-174.

Miyamoto, S. & Kollman, P. A. 1992. SETTLE: An Analytical Version of the SHAKE and RATTLE Algorithms for Rigid Water Models. *J Comput Chem,* 13, 952-962.

Miyazawa, A., Fujiyoshi, Y. & Unwin, N. 2003. Structure and gating mechanism of the acetylcholine receptor pore. *Nature,* 423, 949-55.

Morales-Perez, C. L., Noviello, C. M. & Hibbs, R. E. 2016. X-ray structure of the human alpha 4 beta 2 nicotinic receptor. *Nature,* 538**,** 411-415.

Mowrey, D., Chen, Q., Liang, Y., Liang, J., Xu, Y. & Tang, P. 2013. Signal transduction pathways in the pentameric ligand-gated ion channels. *PLoS One,* 8, e64326.

Murail, S., Wallner, B., Trudell, J. R., Bertaccini, E. & Lindahl, E. 2011. Microsecond simulations indicate that ethanol binds between subunits and could stabilize an open-state model of a glycine receptor. *Biophys J,* 100, 1642-1650.

Naveh, Z. M. H., Malliavin, T. E., Maragliano, L., Cottone, G. & Ciccotti, G. 2014. Conformational Changes in Acetylcholine Binding Protein Investigated by Temperature Accelerated Molecular Dynamics. *PLoS One,* 9, e88555.

Nemecz, A., Hu, H., Fourati, Z., Van Renterghem, C., Delarue, M. & Corringer, P. J. 2017. Full mutational mapping of titratable residues helps to identify proton-sensors involved in the control of channel gating in the Gloeobacter violaceus pentameric ligand-gated ion channel. *PLoS Biol,* 15, e2004470.

Nemecz, A., Prevost, M. S., Menny, A. & Corringer, P. J. 2016. Emerging Molecular Mechanisms of Signal Transduction in Pentameric Ligand-Gated Ion Channels. *Neuron,* 90, 452-470.

Newell, J. G. & Czajkowski, C. 2003. The GABA(A) receptor alpha(1) subunit Pro(174)-Asp(191) segment is involved in GABA binding and channel gating. *J Biol Chem,* 278, 13166-13172.

Newell, J. G., McDevitt, R. A. & Czajkowski, C. 2004. Mutation of glutamate 155 of the GABA(A) receptor beta(2) subunit produces a spontaneously open channel: A trigger for channel activation. *J Neurosci,* 24, 11226-11235.

Ng, H. W., Laughton, C. A. & Doughty, S. W. 2013. Molecular dynamics simulations of the adenosine A2a receptor: structural stability, sampling, and convergence. *J Chem Inf Model,* 53, 1168-1178.

Ngo, V., Stefanovski, D., Haas, S. & Farley, R. A. 2014. Non-equilibrium dynamics contribute to ion selectivity in the KcsA channel. *PLoS One,* 9, e86079.

Ngo, V., Wang, Y., Haas, S., Noskov, S. Y. & Farley, R. A. 2016. K+ Block Is the Mechanism of Functional Asymmetry in Bacterial Na(v) Channels. *PLoS Comput Biol,* 12, e1004482.

Nury, H., Poitevin, F., Van Renterghem, C., Changeux, J. P., Corringer, P. J., Delarue, M. & Baaden, M. 2010. One-microsecond molecular dynamics simulation of channel gating in a nicotinic receptor homologue. *Proc Natl Acad Sci U S A,* 107, 6275-6280.

Nys, M., Kesters, D. & Ulens, C. 2013. Structural insights into Cys-loop receptor function and ligand recognition. *Biochem Pharmacol,* 86, 1042-1053.

Nys, M., Wijckmans, E., Farinha, A., Yoluk, O., Andersson, M., Brams, M., Spurny, R., Peigneur, S., Tytgat, J., Lindahl, E. & Ulens, C. 2016. Allosteric binding site in a Cys-loop receptor ligand-binding domain unveiled in the crystal structure of ELIC in complex with chlorpromazine. *Proc Natl Acad Sci U S A,* 113, E6696-E6703.

Oliveira, A. S., Baptista, A. M. & Soares, C. M. 2011. Inter-domain Communication Mechanisms in an ABC Importer: A Molecular Dynamics Study of the MalFGK2E Complex. *PLoS Comput Biol,* 7, e1002128.

Oliveira, A. S., Damas, J. M., Baptista, A. M. & Soares, C. M. 2014. Exploring O2 diffusion in A-type cytochrome c oxidases: molecular dynamics simulations uncover two alternative channels towards the binuclear site. *PLoS Comput Biol,* 10**,** e1004010.

Oliveira, A. S., Teixeira, V. H., Baptista, A. M. & Soares, C. M. 2005. Reorganization and conformational changes in the reduction of tetraheme cytochromes. *Biophys J,* 89, 3919-3930.

Padgett, C. L. & Lummis, S. C. R. 2008. The F-loop of the GABA(A) receptor gamma(2) subunit contributes to benzodiazepine modulation. *J Biol Chem,* 283, 2702-2708.

Pan, J., Chen, Q., Willenbring, D., Mowrey, D., Kong, X. P., Cohen, A., Divito, C. B., Xu, Y. & Tang, P. 2012a. Structure of the pentameric ligand-gated ion channel GLIC bound with anesthetic ketamine. *Structure,* 20, 1463-1469.

Pan, J., Chen, Q., Willenbring, D., Yoshida, K., Tillman, T., Kashlan, O. B., Cohen, A., Kong, X. P., Xu, Y. & Tang, P. 2012b. Structure of the pentameric ligand-gated ion channel ELIC cocrystallized with its competitive antagonist acetylcholine. *Nat Commun,* 3**,** 1-8.

Paolini, G. V., Ciccotti, G. & van Beijeren, H. 1990. Nonequilibrium molecular dynamics via a nondiverging subtraction technique. *Phys Rev A,* 42, 5912-5916.

Perez, J. J., Tomas, M. S. & Rubio-Martinez, J. 2016. Assessment of the Sampling Performance of Multiple-Copy Dynamics versus a Unique Trajectory. *J Chem Inf Model,* 56, 1950-1962.

Phulera, S., Zhu, H., Yu, J., Claxton, D. P., Yoder, N., Yoshioka, C. & Gouaux, E. 2018. Cryo-EM structure of the benzodiazepine-sensitive alpha1beta1gamma2S tri-heteromeric GABAA receptor in complex with GABA. *Elife,* 7, e39383.

Pless, S. A. & Lynch, J. W. 2009. Ligand-specific Conformational Changes in the alpha 1 Glycine Receptor Ligand-binding Domain. *J Biol Chem,* 284, 15847-15856.

Pless, S. A. & Sivilotti, L. G. 2018. A tale of ligands big and small: An update on how pentameric ligand-gated ion channels interact with agonists and proteins. *Curr Opin Physiol,* 2, 19-26.

Polovinkin, L., Hassaine, G., Perot, J., Neumann, E., Jensen, A. A., Lefebvre, S. N., Corringer, P. J., Neyton, J., Chipot, C., Dehez, F., Schoehn, G. & Nury, H. 2018. Conformational transitions of the serotonin 5-HT3 receptor. *Nature,* 563, 275-279.

Prevost, M. S., Sauguet, L., Nury, H., Van Renterghem, C., Huon, C., Poitevin, F., Baaden, M., Delarue, M. & Corringer, P. J. 2012. A locally closed conformation of a bacterial pentameric proton-gated ion channel. *Nat Struct Mol Biol,* 19, 642-9.

Purohit, P. & Auerbach, A. 2013. Loop C and the mechanism of acetylcholine receptor-channel gating. *J Gen Physiol,* 141, 467-478.

Rovira, J. C., Ballesta, J. J., Vicente-Agullo, F., Campos-Caro, A., Criado, M., Sala, F. & Sala, S. 1998. A residue in the middle of the M2-M3 loop of the beta4 subunit specifically affects gating of neuronal nicotinic receptors. *FEBS Lett,* 433, 89-92.

Roy, J. & Laughton, C. A. 2010. Long-timescale molecular-dynamics simulations of the major urinary protein provide atomistic interpretations of the unusual thermodynamics of ligand binding. *Biophys J,* 99, 218-226.

Rucktooa, P., Haseler, C. A., van Elk, R., Smit, A. B., Gallagher, T. & Sixma, T. K. 2012. Structural characterization of binding mode of smoking cessation drugs to nicotinic acetylcholine receptors through study of ligand complexes with acetylcholine-binding protein. *J Biol Chem,* 287, 23283-23293.

Sali, A. 1995. Comparative Protein Modeling by Satisfaction of Spatial Restraints. *Mol Med Today,* 1, 270-277.

Sauguet, L., Howard, R. J., Malherbe, L., Lee, U. S., Corringer, P. J., Harris, R. A. & Delarue, M. 2013. Structural basis for potentiation by alcohols and anaesthetics in a ligand-gated ion channel. *Nat Commun,* 4, 1697.

Sauguet, L., Shahsavar, A., Poitevin, F., Huon, C., Menny, A., Nemecz, A., Haouz, A., Changeux, J. P., Corringer, P. J. & Delarue, M. 2014. Crystal structures of a pentameric ligand-gated ion channel provide a mechanism for activation. *Proc Natl Acad Sci U S A,* 111, 966-971.

Schmidt, T. H. & Kandt, C. 2012. LAMBADA and InflateGRO2: Efficient Membrane Alignment and Insertion of Membrane Proteins for Molecular Dynamics Simulations. *J Chem Inf Model,* 52, 2657-2669.

Sgrignani, J., Bonaccini, C., Grazioso, G., Chioccioli, M., Cavalli, A. & Gratteri, P. 2009. Insights into docking and scoring neuronal alpha4beta2 nicotinic receptor agonists using molecular dynamics simulations and QM/MM calculations. *J Comput Chem,* 30, 2443-2454.

Shen, X. M., Ohno, K. J., Tsujino, A., Brengman, J. M., Gingold, M., Sine, S. M. & Engel, A. G. 2003. Mutation causing severe myasthenia reveals functional asymmetry of AChR signature cystine loops in agonist binding and gating. *Journal of Clinical Investigation,* 111, 497-505.

Smart, O. S., Neduvelil, J. G., Wang, X., Wallace, B. A. & Sansom, M. S. 1996. HOLE: a program for the analysis of the pore dimensions of ion channel structural models. *J Mol Graph,* 14, 354-360, 376.

Soares, C. M., Baptista, A. M., Pereira, M. M. & Teixeira, M. 2004. Investigation of protonatable residues in Rhodothermus marinus caa_3 haem-copper oxygen reductase: comparison with Paracoccus denitrificans aa_3 haem-copper oxygen reductase. *J Biol Inorg Chem,* 9**,** 124-134.

Spurny, R., Billen, B., Howard, R. J., Brams, M., Debaveye, S., Price, K. L., Weston, D. A., Strelkov, S. V., Tytgat, J., Bertrand, S., Bertrand, D., Lummis, S. C. & Ulens, C. 2013. Multisite binding of a general anesthetic to the prokaryotic pentameric Erwinia chrysanthemi ligand-gated ion channel (ELIC). *J Biol Chem,* 288, 8355-8364.

Spurny, R., Ramerstorfer, J., Price, K., Brams, M., Ernst, M., Nury, H., Verheij, M., Legrand, P., Bertrand, D., Bertrand, S., Dougherty, D. A., de Esch, I. J., Corringer, P. J., Sieghart, W., Lummis, S. C. & Ulens, C. 2012. Pentameric ligand-gated ion channel ELIC is activated by GABA and modulated by benzodiazepines. *Proc Natl Acad Sci U S A,* 109, E3028-E3034.

Stock, G. & Hamm, P. 2018. A non-equilibrium approach to allosteric communication. *Philos Trans R Soc Lond B Biol Sci,* 373, 2170187

Suresh, A. & Hung, A. 2016. Molecular simulation study of the unbinding of alpha-conotoxin [Upsilon4E]GID at the alpha7 and alpha4beta2 neuronal nicotinic acetylcholine receptors. *J Mol Graph Model,* 70, 109-121.

Tavares Xda, S., Blum, A. P., Nakamura, D. T., Puskar, N. L., Shanata, J. A., Lester, H. A. & Dougherty, D. A. 2012. Variations in binding among several agonists at two stoichiometries of the neuronal, alpha4beta2 nicotinic receptor. *J Am Chem Soc,* 134, 11474-11480.

Teixeira, V. H., Cunha, C. A., Machuqueiro, M., Oliveira, A. S., Victor, B. L., Soares, C. M. & Baptista, A. M. 2005. On the use of different dielectric constants for computing individual and pairwise terms in poisson-boltzmann studies of protein ionization equilibrium. *J Phys Chem B,* 109**,** 14691-706.

Teixeira, V. H., Soares, C. M. & Baptista, A. M. 2002. Studies of the reduction and protonation behavior of tetraheme cytochromes using atomic detail. *J Biol Inorg Chem,* 7, 200-216.

Thompson, A. J., Lester, H. A. & Lummis, S. C. 2010. The structural basis of function in Cys-loop receptors. *Q Rev Biophys,* 43, 449-499.

Thompson, A. J., Padgett, C. L. & Lummis, S. C. R. 2006. Mutagenesis and molecular modeling reveal the importance of the 5-HT3 receptor F-loop. *J Biol Chem,* 281, 16576-16582.

Timmermann, D. B., Gronlien, J. H., Kohlhaas, K. L., Nielsen, E. O., Dam, E., Jorgensen, T. D., Ahring, P. K., Peters, D., Holst, D., Christensen, J. K., Malysz, J., Briggs, C. A., Gopalakrishnan, M. & Olsen, G. M. 2007. An allosteric modulator of the alpha7 nicotinic acetylcholine receptor possessing cognition-enhancing properties in vivo. *J Pharmacol Exp Ther,* 323, 294-307.

Ulens, C., Akdemir, A., Jongejan, A., van Elk, R., Bertrand, S., Perrakis, A., Leurs, R., Smit, A. B., Sixma, T. K., Bertrand, D. & de Esch, I. J. 2009. Use of acetylcholine binding protein in the search for novel alpha7 nicotinic receptor ligands. In silico docking, pharmacological screening, and X-ray analysis. *J Med Chem,* 52, 2372-2383.

Ulens, C., Spurny, R., Thompson, A. J., Alqazzaz, M., Debaveye, S., Han, L., Price, K., Villalgordo, J. M., Tresadern, G., Lynch, J. W. & Lummis, S. C. 2014. The prokaryote ligand-gated ion channel ELIC captured in a pore blocker-bound conformation by the Alzheimer's disease drug memantine. *Structure,* 22, 1399-407.

Unwin, N. 2013. Nicotinic acetylcholine receptor and the structural basis of neuromuscular transmission: insights from Torpedo postsynaptic membranes. *Q Rev Biophys,* 46, 283-322.

Unwin, N. & Fujiyoshi, Y. 2012. Gating Movement of Acetylcholine Receptor Caught by Plunge-Freezing. *J Mol Biol,* 422, 617-634.

Van Arnam, E. B. & Dougherty, D. A. 2014. Functional probes of drug-receptor interactions implicated by structural studies: Cys-loop receptors provide a fertile testing ground. *J Med Chem,* 57, 6289-6300.

Van Der Spoel, D., Lindahl, E., Hess, B., Groenhof, G., Mark, A. E. & Berendsen, H. J. 2005. GROMACS: fast, flexible, and free. *J Comput Chem,* 26, 1701-1718.

Walsh, R. M., Jr., Roh, S. H., Gharpure, A., Morales-Perez, C. L., Teng, J. & Hibbs, R. E. 2018. Structural principles of distinct assemblies of the human alpha4beta2 nicotinic receptor. *Nature,* 557, 261-265.

Wells, S. A., van der Kamp, M. W., McGeagh, J. D. & Mulholland, A. J. 2015. Structure and Function in Homodimeric Enzymes: Simulations of Cooperative and Independent Functional Motions. *PLoS One,* 10, e0133372.

Willenbring, D., Xu, Y. & Tang, P. 2010. The role of structured water in mediating general anesthetic action on alpha4beta2 nAChR. *Phys Chem Chem Phys,* 12, 10263-10269.

Woods, C. J., Malaisree, M., Long, B., McIntosh-Smith, S. & Mulholland, A. J. 2013. Computational assay of H7N9 influenza neuraminidase reveals R292K mutation reduces drug binding affinity. *Sci Rep,* 3, 3561.

Yang, S. S. & Smetena, I. 1995. Evaluation of Capillary Electrophoresis for the Analysis of Nicotine and Selected Minor Alkaloids from Tobacco. *Chromatographia,* 40, 375-378.

Yoluk, O., Lindahl, E. & Andersson, M. 2015. Conformational Gating Dynamics in the GluCl Anion-Selective Chloride Channel. *Acs Chemical Neuroscience,* 6, 1459-1467.

Yu, R., Hurdiss, E., Greiner, T., Lape, R., Sivilotti, L. & Biggin, P. C. 2014. Agonist and antagonist binding in human glycine receptors. *Biochemistry,* 53, 6041-6051.

Zhu, F. & Hummer, G. 2010. Pore opening and closing of a pentameric ligand-gated ion channel. *Proc Natl Acad Sci U S A,* 107, 19814-19819.

Zhu, S., Noviello, C. M., Teng, J., Walsh, R. M., Jr., Kim, J. J. & Hibbs, R. E. 2018. Structure of a human synaptic GABAA receptor. *Nature,* 559, 67-72.

Zimmermann, I. & Dutzler, R. 2011. Ligand activation of the prokaryotic pentameric ligand-gated ion channel ELIC. *PLoS Biol,* 9, e1001101.

Zimmermann, I., Marabelli, A., Bertozzi, C., Sivilotti, L. G. & Dutzler, R. 2012. Inhibition of the prokaryotic pentameric ligand-gated ion channel ELIC by divalent cations. *PLoS Biol,* 10, e1001429.

Zwart, R., De Filippi, G., Broad, L. M., McPhie, G. I., Pearson, K. H., Baldwinson, T. & Sher, E. 2002. 5-Hydroxyindole potentiates human alpha 7 nicotinic receptor-mediated responses and enhances acetylcholine-induced glutamate release in cerebellar slices. *Neuropharmacology,* 43, 374-384.

Figure 1

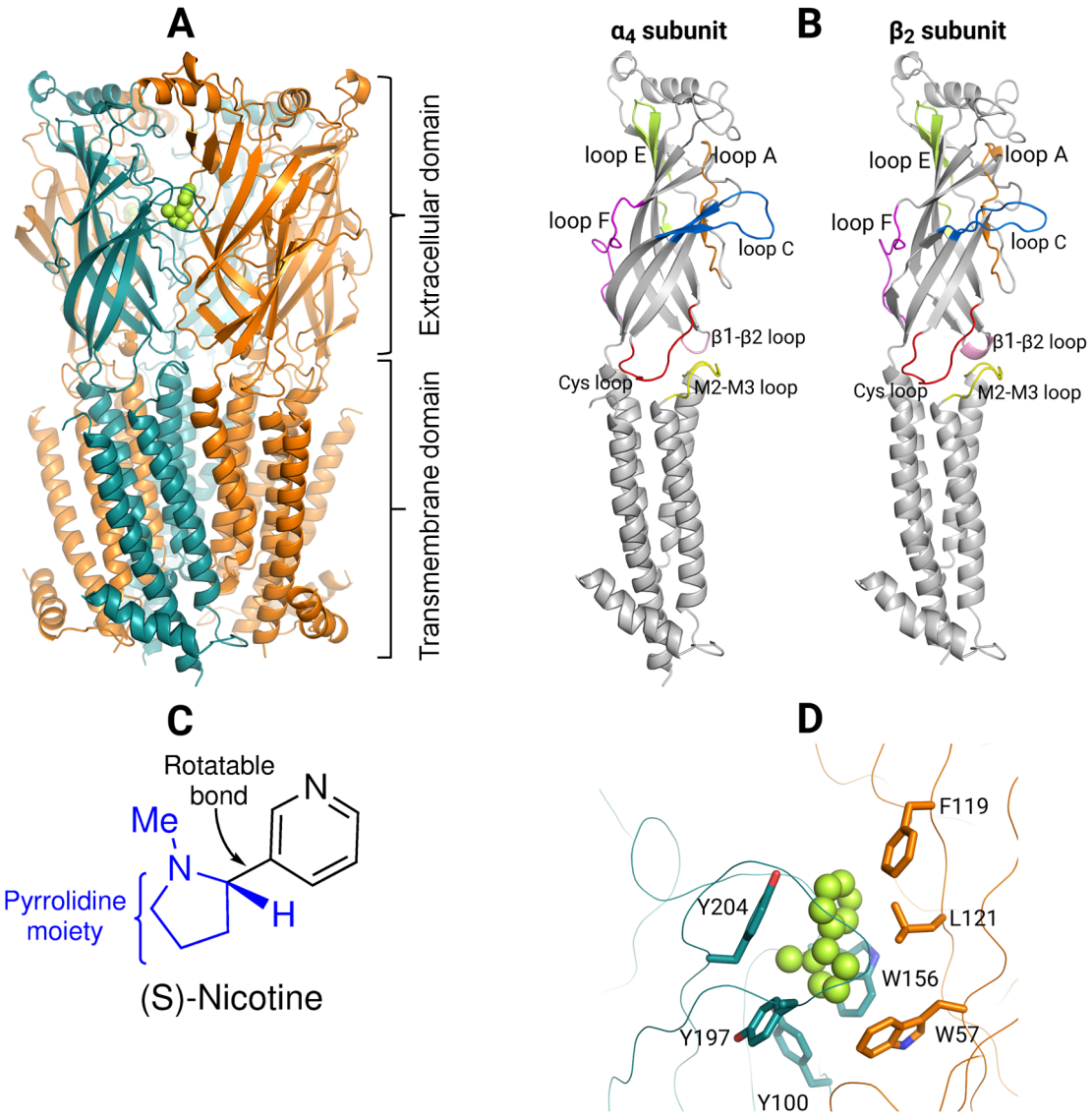
A
Extracellular domain
Transmembrane domain
B
α4 subunit
β2 subunit
loop E
loop A
loop F
loop C
β1-β2 loop
Cys loop
M2-M3 loop
C
Rotatable bond
N
Me
N
H
Pyrrolidine moiety
(S)-Nicotine
D
F119
Y204
L121
W156
Y197
W57
Y100

Figure 2

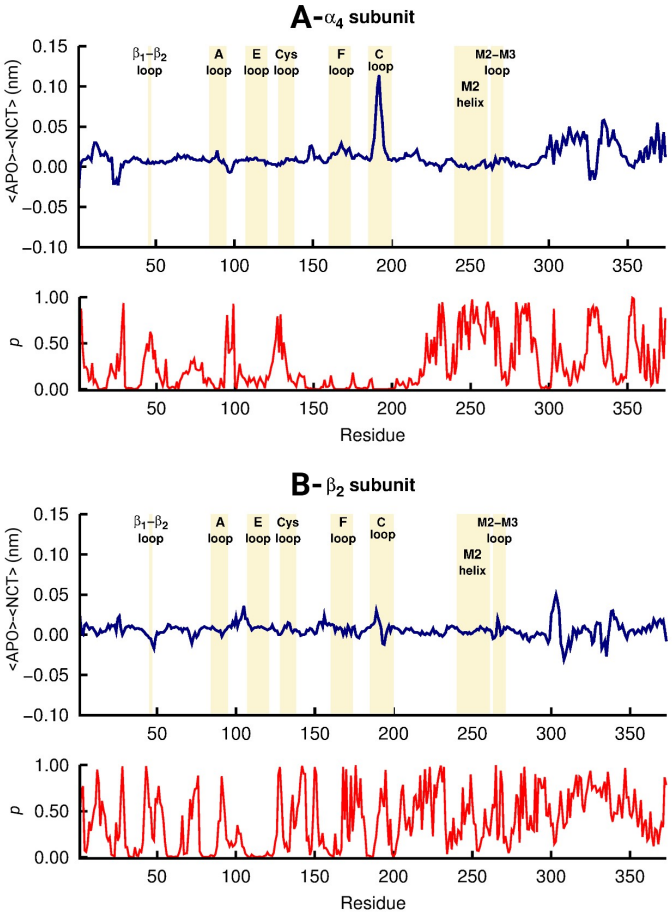
A-α4 subunit
β1–β2 loop
A loop
E loop
Cys loop
F loop
C loop
M2–M3 loop
M2 helix
<APO>–<NCT> (nm)
p
Residue
B-β2 subunit
β1–β2 loop
A loop
E loop
Cys loop
F loop
C loop
M2–M3 loop
M2 helix
<APO>–<NCT> (nm)
p
Residue


C

Figure 3

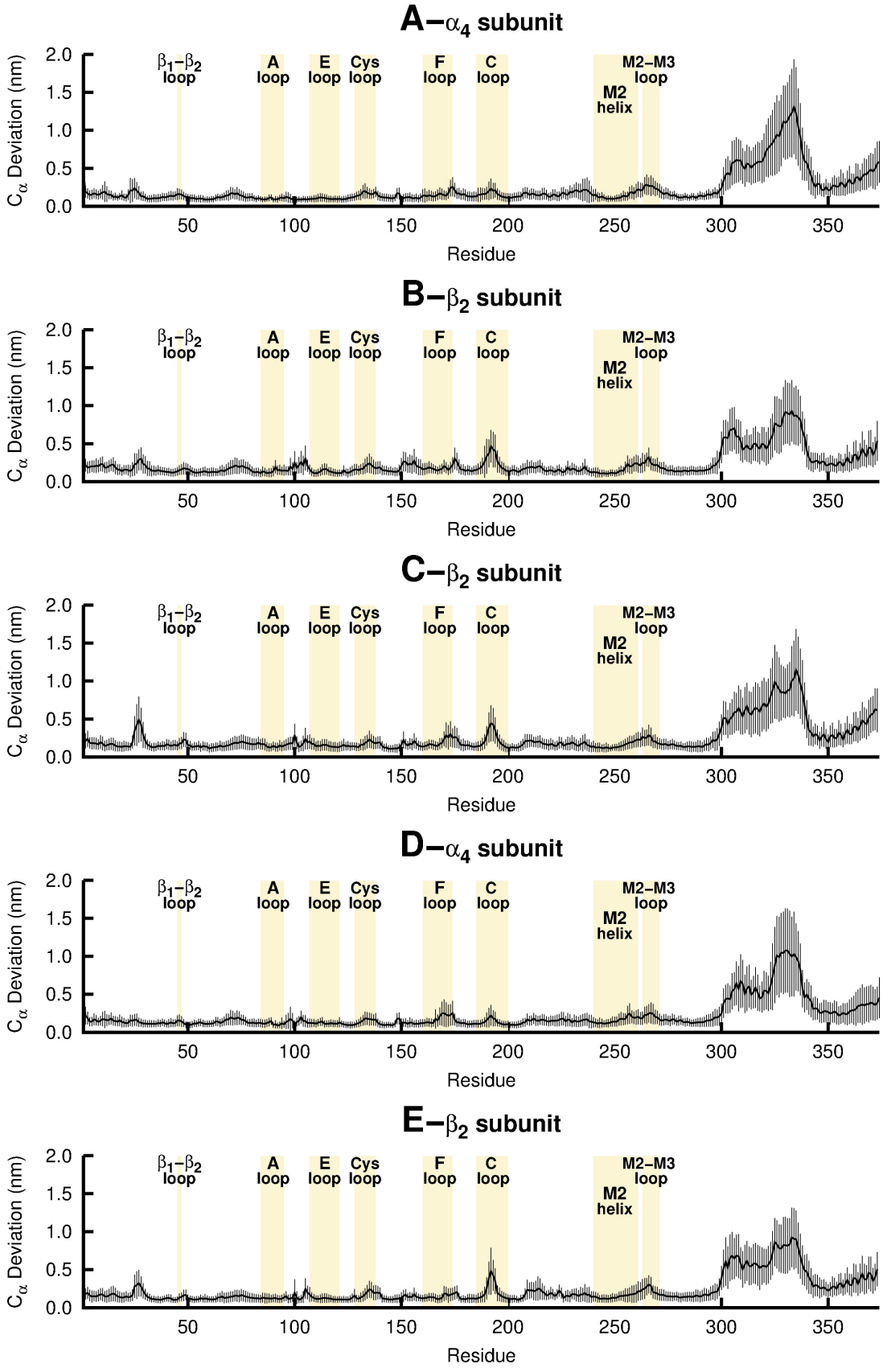
A–α4 subunit
B–β2 subunit
C–β2 subunit
D–α4 subunit
E–β2 subunit
Cα Deviation (nm)
Residue
β1–β2 loop
A loop
E loop
Cys loop
F loop
C loop
M2 helix
M2–M3 loop
0.0
0.5
1.0
1.5
2.0
50
100
150
200
250
300
350

Figure 4

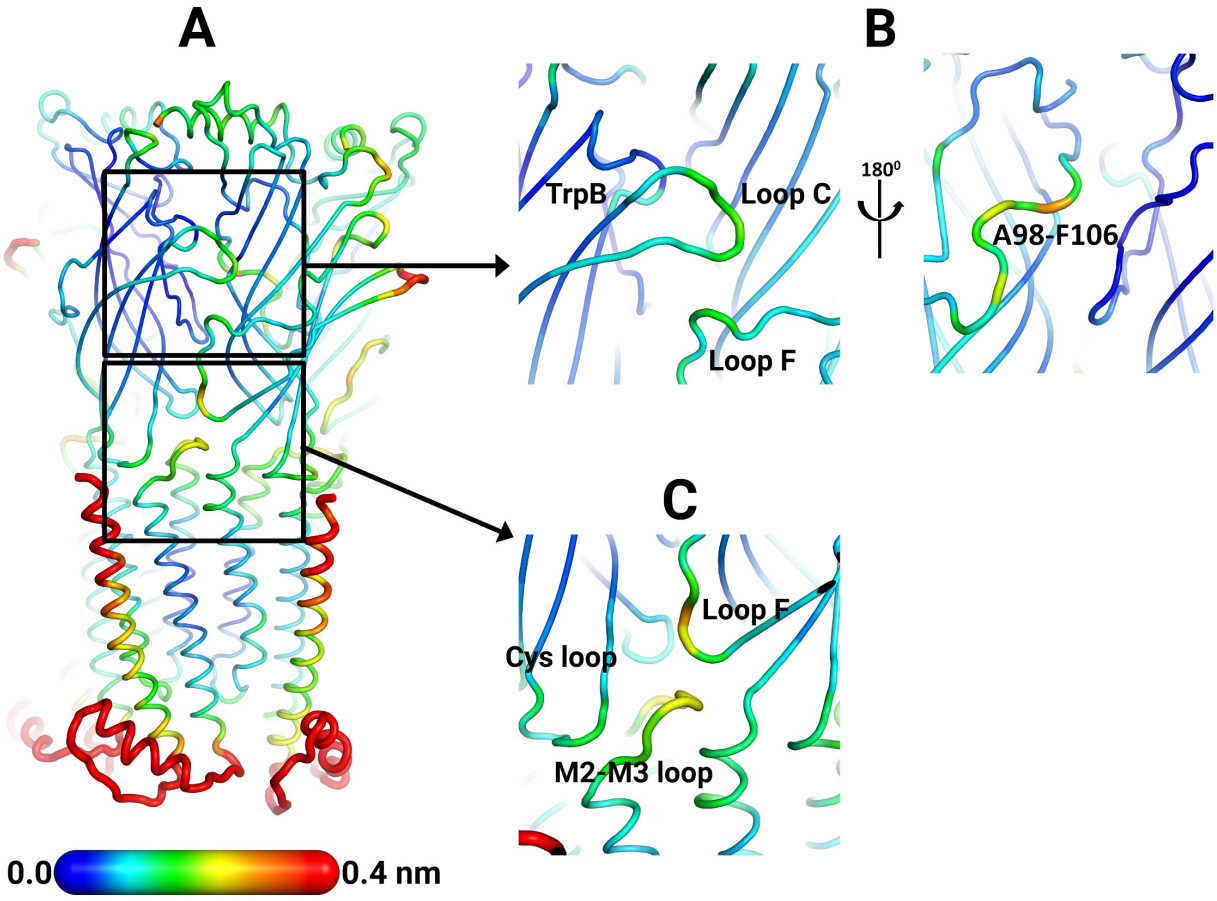
A
B
C
TrpB
Loop C
Loop F
180⁰
A98-F106
Loop F
Cys loop
M2-M3 loop
0.0
0.4 nm

Figure 5

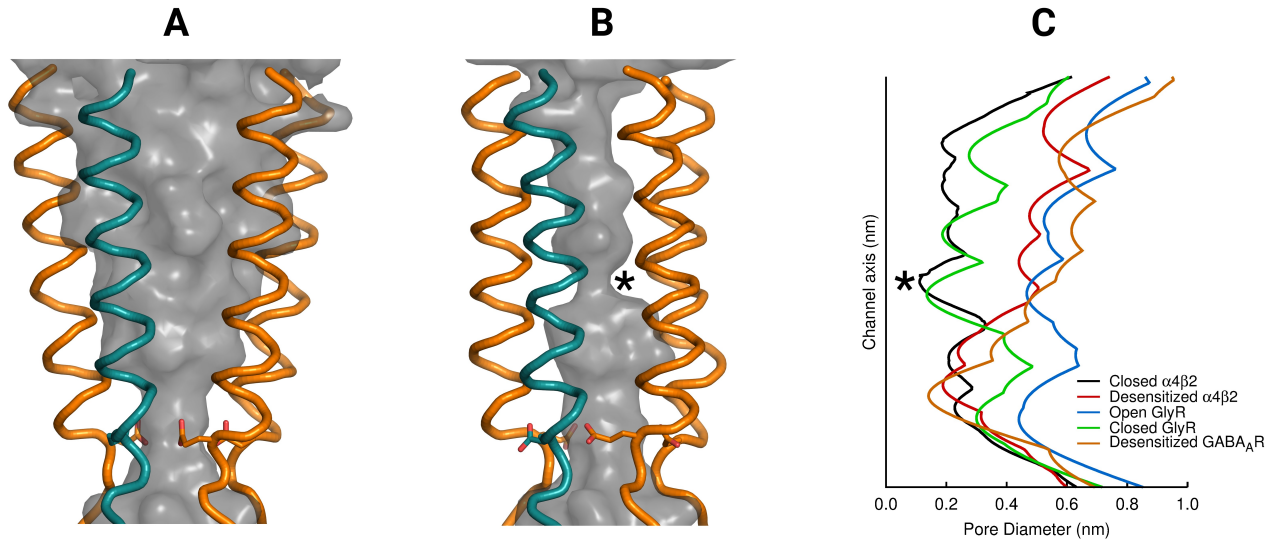
A
B
C
*
*
Channel axis (nm)
Pore Diameter (nm)
0.0
0.2
0.4
0.6
0.8
1.0
Closed α4β2
Desensitized α4β2
Open GlyR
Closed GlyR
Desensitized GABA$_A$R

Figure 6

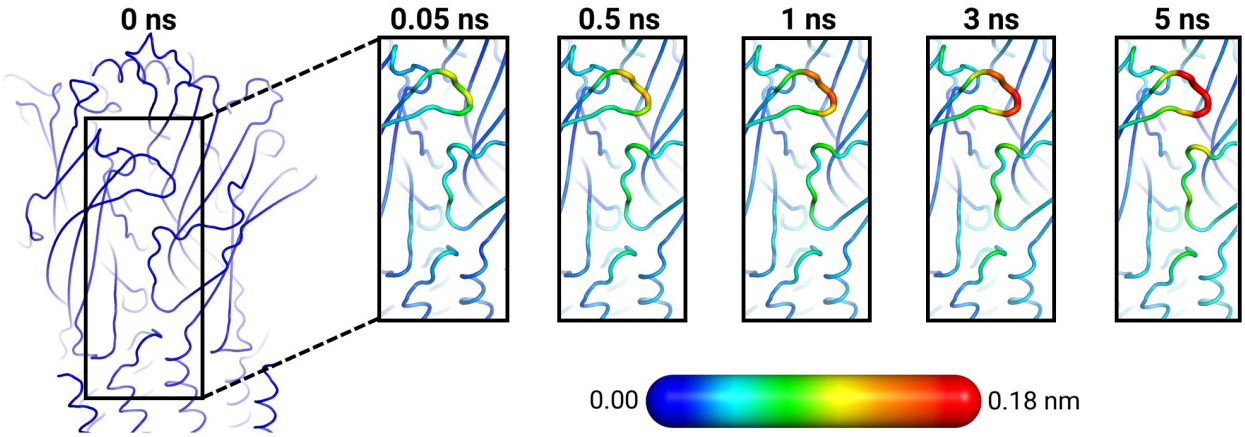

Figure 7

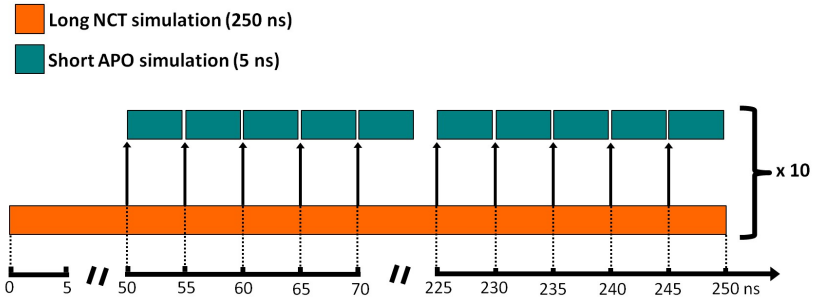
Long NCT simulation (250 ns)
Short APO simulation (5 ns)
x 10
0
5
50
55
60
65
70
225
230
235
240
245
250 ns